Vibrational Analysis of the *all-trans*-Retinal Chromophore in Light-Adapted Bacteriorhodopsin

Steven O. Smith,[1a,c] Mark S. Braiman,[1a,d] Anne B. Myers,[1a,e] Johannes A. Pardoen,[1b] Jacques M. L. Courtin,[1b] Chris Winkel,[1b] Johan Lugtenburg,[1b] and Richard A. Mathies*[1a]

Contribution from the Departments of Chemistry, University of California, Berkeley, California 94720, and Leiden University, 2300 RA Leiden, The Netherlands.
Received May 27, 1986

Abstract: Resonance Raman spectra of light-adapted bacteriorhodopsin (BR_{568}) have been obtained using purple membrane regenerated with isotopic retinal derivatives. The chromophore was labeled with ^{13}C at positions 5, 6, 7, 8, 9, 10, 11, 12, 13, 14, and 15, while deuterium substitutions were made at positions 7, 8, 10, 11, 12, 14, and 15 and on the Schiff base nitrogen. On the basis of the observed isotopic shifts, empirical assignments have been made for the vibrations observed between 700 and 1700 cm^{-1}. A modified Urey–Bradley force field has been refined to satisfactorily reproduce the vibrational frequencies and isotopic shifts. Of particular importance is the assignment of the normal modes in the structurally sensitive 1100–1300 cm^{-1} "fingerprint region" to specific combinations of C–C stretching and CCH rocking motions. The methyl-substituted "C_8–C_9" and "C_{12}–C_{13}" stretches are highest in frequency at 1214 and 1248–1255 cm^{-1}, respectively, as a result of coupling with their associated C–methyl stretches. The C_8–C_9 and C_{12}–C_{13} stretches also couple strongly with the $C_{10}H$ and $C_{14}H$ rocks, respectively. The 1169-cm^{-1} mode is assigned as a relatively localized C_{10}–C_{11} stretch, and the 1201-cm^{-1} mode is a localized C_{14}–C_{15} stretch. The frequency ordering and spacing of the C–C stretches in BR_{568} is the same as that observed in the *all-trans*-retinal protonated Schiff base. However, each vibration is ~10 cm^{-1} higher in the pigment as a result of increased π-electron delocalization. The frequencies and Raman intensities of the normal modes are compared with the predictions of theoretical models for the ground- and excited-state structure of the retinal chromophore in bacteriorhodopsin.

Chemical reactions that occur in the active sites of biological macromolecules such as enzymes, photosynthetic pigments, and heme proteins often involve rapid changes in the structure of transiently bound substrate molecules or covalently bound prosthetic groups. Vibrational spectroscopy is a powerful method for studying the molecular changes involved in these reactions since the frequencies and intensities of the vibrational normal modes of an enzyme substrate or prosthetic group are sensitive to both molecular structure and environment. Resonance Raman spectroscopy is a useful technique for obtaining vibrational spectra of specific chromophoric groups within proteins. By selecting a laser excitation wavelength within the absorption band of retinal pigments or heme proteins, it is possible to selectively enhance the chromophore resonances over the more numerous protein vibrations.[2,3] Furthermore, the use of pulsed laser techniques can provide picosecond time-resolution, sufficient to monitor very fast biochemical reactions.[4] Fourier transform infrared (FTIR) difference spectroscopy offers a second approach for obtaining spectra of reactive groups in macromolecules.[5] In both the Raman and FTIR techniques, interpreting the changes in vibrational spectra in terms of molecular structure or environment requires the assignment of the vibrational lines to specific normal modes.

Bacteriorhodopsin (BR), a 26 000-dalton protein in the "purple membrane" of *Halobacterium halobium*, is an example of a protein whose structure and function can be probed by vibrational spectroscopy.[6] Light absorption by its retinal prosthetic group (see Figure 1) drives the light-adapted form of this pigment, BR_{568}, through a cyclic photochemical reaction[7] which results in the transport of protons across the bacterial cell membrane. We are interested in identifying the features in the vibrational spectrum that are characteristic of the structure of the retinal chromophore, as well as learning how retinal's protein environment modifies chromophore structure to make BR an efficient light-energy convertor. This requires detailed vibrational assignments for the *all-trans*-retinal model compounds as well as for the protein-bound chromophore. The vibrational analyses of *all-trans*-retinal (ATR)[8] and more recently the *all-trans*-retinal protonated Schiff base (PSB)[9] have brought this goal closer to realization. However, a complete vibrational analysis has not yet been performed for any retinal-containing *pigment*. A detailed vibrational analysis of BR_{568} is needed to learn more about its structure and function and to provide a basis for the interpretation of the vibrational spectra of other retinal-containing pigments.

In this paper, we present the vibrational assignments of light-adapted bacteriorhodopsin based on an extensive set of ^{13}C- and ^{2}H-labeled derivatives. Specific isotopic substitution of the retinal chromophore provides a direct method for assigning its normal modes. This approach has permitted one of the most detailed analyses to date of the vibrational structure of a protein-bound chromophore. Comparison of the BR_{568} spectral assignments with those of the *all-trans* protonated Schiff base indicates that many of the vibrational features that are characteristic of an *all-trans* structure are observed in the pigment with only slight differences due to bacteriorhodopsin's more delocalized electronic structure. The vibrational analysis of BR_{568} is discussed in the light of recent NMR[10] and optical results[11,12] on the

(1) (a) University of California, Berkeley. (b) Leiden University. (c) Current address: Francis Bitter National Magnet Laboratory, Massachusetts Institute of Technology, Cambridge, MA. (d) Current address: Physics Department, Boston University, Boston, MA. (e) Current address: Department of Chemistry, University of Rochester, Rochester, NY.

(2) For reviews on Raman studies of enzymes and heme proteins see: (a) Carey, P. R.; Storer, A. C. *Annu. Rev. Biophys. Bioeng.* **1984**, *13*, 25. (b) Spiro, T. G. In *Advances in Protein Chemistry*; Anfinsen, C. B., Edsall, J. T., Richards, F. M., Eds.; Academic Press: New York, 1985; Vol. 37, p 111.

(3) For reviews on Raman studies of rhodopsins see: (a) Mathies, R. A.; Smith, S. O.; Palings, I. In *Biological Applications of Raman Spectroscopy*; Spiro, T. G., Ed.; Wiley-Interscience: New York, 1987; Vol. 2, p 59. (b) Smith, S. O.; Lugtenburg, J.; Mathies, R. A. *J. Memb. Biol.* **1985**, *85*, 95. (c) Stockburger, M.; Alshuth, T.; Oesterhelt, D.; Gärtner, W. *Adv. Infrared Raman Spectrosc.* **1986**, *13*, 483. (d) Warshel, A. *Annu. Rev. Biophys. Bioeng.* **1977**, *6*, 273. (e) Callender, R.; Honig, B. *Annu. Rev. Biophys. Bioeng.* **1977**, *6*, 33.

(4) Terner, J.; El-Sayed, M. A. *Acc. Chem. Res.* **1985**, *18*, 331.

(5) (a) Rothschild, K. J.; Roepe, P.; Lugtenburg, J.; Pardoen, J. A. *Biochemistry* **1984**, *23*, 6103. (b) Bagley, K. A.; Balogh-Nair, V.; Croteau, A. A.; Dollinger, G.; Ebrey, T. G.; Eisenstein, L.; Hong, M. K.; Nakanishi, K.; Vittitow, J. *Biochemistry* **1985**, *24*, 6055. (c) Engelhard, M.; Gerwert, K.; Hess, B.; Kreutz, W.; Siebert, F. *Biochemistry* **1985**, *24*, 400.

(6) For bacteriorhodopsin reviews see: (a) Birge, R. R. *Annu. Rev. Biophys. Bioeng.* **1981**, *10*, 315. (b) Stoeckenius, W.; Bogomolni, R. A. *Annu. Rev. Biochem.* **1982**, *51*, 587.

(7) Lozier, R. H.; Bogomolni, R. A.; Stoeckenius, W. *Biophys. J.* **1975**, *15*, 955.

(8) Curry, B.; Broek, A.; Lugtenburg, J.; Mathies, R. *J. Am. Chem. Soc.* **1982**, *104*, 5274.

(9) Smith, S. O.; Myers, A. B.; Mathies, R. A.; Pardoen, J. A.; Winkel, C.; van den Berg, E. M. M.; Lugtenburg, J. *Biophys. J.* **1985**, *47*, 653.

0002-7863/87/1509-3108$01.50/0

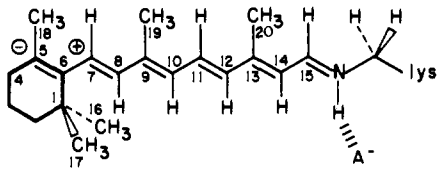

Figure 1. Structure of the protonated retinal Schiff base chromophore in light-adapted bacteriorhodopsin. Solid-state ^{13}C NMR and retinal analogue studies have shown that the protein-bound chromophore adopts the 6-*s*-*trans* conformation.[10,41] The chromophore interacts with a protein dipole near C_5–C_7 and has a weakened hydrogen-bonding interaction with its counterion A^-.[10-12]

structure of the retinal chromophore in BR_{568}, and the Raman frequencies and intensities are compared with the predictions of current models for the structure and photochemistry of bacteriorhodopsin.

Experimental Section

The ^{13}C- and ^2H-labeled derivatives of retinal were synthesized according to published procedures.[13] The isomeric purity was ≥98% as determined by high-performance liquid chromatography. The isotopic purity was ≥98% for each position deuteriated and ≥92% for each position labeled with ^{13}C based on mass spectrometric analysis.

Bacterioopsin was isolated and purified from a retinal deficient strain of *H. halobium* (JW5) and regenerated with isotopically labeled retinals as described in ref 14. In the case of the 10-D, 11-D, 12-D, and 11,12-D_2 derivatives, regeneration of hydroxylamine-bleached purple membrane was used to obtain isotopically labeled purple membrane.[15] Raman spectra of bacterioopsin regenerated with use of the two procedures are identical.[16]

Raman spectra of light-adapted bacteriorhodopsin were obtained with use of a rapid-flow technique.[17] The purple membrane suspension was recirculated from a reservoir which was maintained at 10 °C and illuminated with an incandescent light to keep the sample in the light-adapted state. The flow speed of the sample (300 cm/s) and the laser power at 514.5 nm (30 mW cylindrically focused, focal length = 3.7 cm) were adjusted to control photoreaction of the pigment as the sample crossed the laser beam. The photoalteration parameter[18] was calculated to be ≤0.1 on the basis of a molar extinction of BR_{568} at 514.5 nm of 35 000 M^{-1} cm^{-1} and a quantum yield for photochemical reaction of 0.3.[7,19] This corresponds to less than 10% photolysis of the sample as it passes through the laser beam. The purple membrane solutions were buffered in distilled water at pH 7 with 10 mM HEPES, and typical sample volumes were ~25 mL with an absorbance of 1–2 at 570 nm (1 cm path length). Raman spectra of the *all-trans*-PSB were obtained of microcrystalline precipitates with use of 752-nm laser excitation as previously described.[9]

The Raman apparatus consisted of a Spex 1401 double monochromator with a Spex 1419 illuminator and photon counting detection (PAR 1105/1120). The monochromator was stepped in 2-cm^{-1} increments and the spectral resolution was ~3.4 cm^{-1} for the ^{13}C derivatives and 4–5 cm^{-1} for the ^2H derivatives. Data were averaged, smoothed (three point sliding average), and corrected for detector sensitivity. Fluorescence backgrounds (simulated by a quartic polynomial) were subtracted with a PDP 11/23 computer.

Computational Methods. Normal mode calculations were performed with use of the Wilson FG method.[20] The atomic coordinates for the 6-*s*-*trans*, C_{15}-*anti* *all-trans* protonated Schiff base were calculated with use of the QCFF-π method.[21] Solid-state NMR studies have shown that the protein-bound chromophore adopts the planar C_6–C_7 *s*-*trans* conformation,[10] and NMR and Raman experiments indicate that the C=N bond is in the *trans* (or *anti*) configuration[22] as depicted in Figure 1. The methyl groups were made tetrahedral to allow the transfer of force constants developed for small model polyenes, and they were rotated to give reflection symmetry in the plane of the polyene chain. Also, the structure was truncated by replacing carbons 1, 4, and 18 of the ionone ring and the δ-carbon of the lysine group with atoms that have a mass of 15, a valence of 1, and the default potential parameters of an sp^3 carbon.

The final force field for BR_{568} is given in Table I. We began with the force field developed to fit the Raman frequencies of the *all-trans*-retinylidine *n*-butylamine PSB.[9] The *all-trans*-PSB force constants which were iterated to produce the BR_{568} force field are included in parentheses in Table I. For coordinate pairs whose geometric relationship changes as a result of *cis*–*trans* isomerization about the C_6–C_7 bond, the appropriate bend–bend and bend–stretch interaction constants were changed to values derived from studies on configurational isomers, small molecules, and retinal model compounds.[23]

For the in-plane vibrations, the stretching and hydrogen bending force constants, along with selected off-diagonal coupling constants, were iteratively adjusted to obtain the best fit to the experimental frequencies of native BR and 16 of its isotopic derivatives (*N*-D; 15-D; 14-D; 12-D; 11-D; 10-D; 8-D; 7-D; 14,15-^{13}C; 13-^{13}C; 12-^{13}C; 10,11-^{13}C; 9-^{13}C; 8-^{13}C; 7-^{13}C; and 6-^{13}C). These derivatives incorporate ^{13}C and ^2H labels at key positions along the retinal chain and were the minimum set necessary for successful refinement of the force field. For the out-of-plane vibrations, the diagonal wag and selected off-diagonal wag–wag interaction constants were iterated to obtain the best fit to the experimental frequencies of native BR and eleven isotopic derivatives (*N*-D; 15-D; 15,*N*-D_2; 14-D; 14,*N*-D_2; 12-D; 11-D; 11,12-D_2; 10-D; 8-D; and 7D). Experimental frequencies corresponding to vibrations localized on the methyl groups were not included in the force constant refinement. The final force field in Table I was refined to fit 231 in-plane frequencies of native BR and 16 isotopic derivatives with a root-mean-square error of 4.9 cm^{-1} (maximum error 17 cm^{-1}) and 68 out-of-plane frequencies of native BR and 11 isotopic derivatives with a root-mean-square error of 6.3 cm^{-1} (maximum error 19 cm^{-1}). In addition, the final force field fit the 274 CC stretching and CCH rocking frequencies of 20 other isotopic derivatives which were not used in the refinement (e.g., 14,15-D_2-, 12,14-D_2-, and 7,8-D_2-BR_{568}) with a root-mean-square error of 5.7 cm^{-1} (maximum error 19 cm^{-1}). The molecular geometry and the complete force field are available in the supplementary material.

Results

The observed Raman lines of BR_{568} can be roughly divided into four groups: the C=C stretches (1500–1600 cm^{-1}), the CCH in-plane rocks (1250–1400 cm^{-1}), the C–C stretches (1100–1250 cm^{-1}), and the hydrogen out-of-plane (HOOP) wags (700–1000 cm^{-1}). We first discuss the assignments of these four vibrational groups and then separately discuss the normal modes associated with the methyl groups and the cyclohexene ring. The calculated normal modes and assignments for native BR_{568} are given in Table II.

(A) In-Plane Chain Vibrations. C=C Stretches. The retinal chromophore in BR_{568} has five C=C stretching internal coordinates that contribute primarily to vibrations in the 1500–

(10) Harbison, G. S.; Smith, S. O.; Pardoen, J. A.; Courtin, J. M. L.; Lugtenburg, J.; Herzfeld, J.; Mathies, R. A.; Griffin, R. G. *Biochemistry* **1985**, *24*, 6955.

(11) Lugtenburg, J.; Muradin-Szweykowska, M.; Heeremans, C.; Pardoen, J. A.; Harbison, G. S.; Herzfeld, J.; Griffin, R. G.; Smith, S. O.; Mathies, R. A. *J. Am. Chem. Soc.* **1986**, *108*, 3104.

(12) Spudich, J. L.; McCain, D. A.; Nakanishi, K.; Okabe, M.; Shimizu, N.; Rodman, H.; Honig, B.; Bogomolni, R. A. *Biophys. J.* **1986**, *49*, 479.

(13) (a) Lugtenburg, J. *Pure Appl. Chem.* **1985**, *57*, 753. (b) Lugtenburg, J. *Spectroscopy of Biological Molecules*; Reidel: Boston; NATO ASI Series C, 139, pp 447–455. (c) Courtin, J. M. L.; 't Lam, G. K.; Peters, A. J. M.; Lugtenburg, J. *Recl. Trav. Chim. Pays-Bas* **1985**, *104*, 281. (d) Pardoen, J. A.; van den Berg, E. M. M.; Winkel, C.; Lugtenburg, J. *Recl. Trav. Chim. Pays-Bas* **1986**, *105*, 92. (e) Pardoen, J. A.; Mulder, P. P. J.; van den Berg, E. M. M.; Lugtenburg, J. *Can. J. Chem.* **1985**, *63*, 1431.

(14) Smith, S. O.; Pardoen, J. A.; Mulder, P. P. J.; Curry, B.; Lugtenburg, J.; Mathies, R. *Biochemistry* **1983**, *22*, 6141.

(15) Braiman, M. S. Ph.D. Dissertation, 1983, University of California, Berkeley.

(16) Smith, S. O. Ph.D. Dissertation, 1985, University of California, Berkeley.

(17) Braiman, M.; Mathies, R. *Biochemistry* **1980**, *19*, 5421.

(18) Mathies, R.; Oseroff, A. R.; Stryer, L. *Proc. Natl. Acad. Sci. U.S.A.* **1976**, *73*, 1.

(19) Goldschmidt, C. R.; Ottolenghi, M.; Korenstein, R. *Biophys. J.* **1976**, *16*, 839.

(20) Wilson, E. B.; Decius, J. C.; Cross, P. C. *Molecular Vibrations*; McGraw-Hill: New York, 1955.

(21) Warshel, A.; Karplus, M. *J. Am. Chem. Soc.* **1974**, *96*, 5677.

(22) (a) Smith, S. O.; Myers, A. B.; Pardoen, J. A.; Winkel, C.; Mulder, P. P. J.; Lugtenburg, J.; Mathies, R. *Proc. Natl. Acad. Sci. U.S.A.* **1984**, *81*, 2055. (b) Harbison, G. S.; Smith, S. O.; Pardoen, J. A.; Winkel, C.; Lugtenburg, J.; Herzfeld, J.; Mathies, R.; Griffin, R. G. *Proc. Natl. Acad. Sci. U.S.A.* **1984**, *81*, 1706.

(23) Curry, B. Ph.D. Dissertation, 1982, University of California, Berkeley. The coordinates in the BR_{568} force field affected by isomerization about the C_6–C_7 bond and their 6-*s*-*trans* values are the following: $h(R_{18}C_5C_6,C_5C_6C_7)$, 0.338; $h(R_1C_6C_7,C_6C_7C_8)$, 0.338; $h(R_1C_6C_7,C_6C_7H)$, 0.076; h-$(R_4C_5C_6,C_5C_6C_7)$, 0.032; $h(C_5C_6C_7,C_6C_7C_8)$, $h(C_6C_7C_8,C_7C_8C_9)$, 0.112. In addition, the $m(C_6$–$C_7,C_6C_5R_4)$, $m(C_6$–$C_7,C_7C_8C_9)$, $m(C_6$–$C_7,C_6C_5R_{18})$, and $m(C_6$–$C_7,C_7C_8H)$ interaction constants change sign.

Table I. Modified Urey–Bradley Force Field for BR_{568}[a]

coordinate	force constant	coordinate	force constant	coordinate	force constant
Chain Stretches		Urey–Bradley		Out-of-Plane	
K(5=6)	7.04 (6.40)	F(C=CH)	0.52	H(7w)	0.520
K(7=8)	6.79 (6.56)	F(C—CH)	0.49	H(8w)	0.494
K(9=10)	6.10 (6.34)	F(CCC)	0.35	H(10w)	0.475
K(11=12)	5.80 (6.22)	F(RCR)	0.59	H(11w)	0.476
K(13=14)	6.27 (6.20)	F(RCC)	0.59	H(12w)	0.480
K(C=N)	7.80 (7.85)	F(RCH)	0.55	H(14w)	0.450
K(6—7)	2.58 (3.57)	F(N=CH)	0.85 (0.80)	H(15w)	0.553
K(8—9)	3.70 (3.48)	F(C=NH)	0.50 (0.30)	H(Nw)	0.386
K(10—11)	3.92 (3.86)	F(C—NH)	0.55	H(CH_3)	0.570
K(12—13)	4.51 (4.13)	F(N—CH)	0.48	t(C—C)	0.197
K(14—15)	4.21 (4.01)	F(CC=N)	0.80	t(C=C)	0.545
K(C—R)	2.55 (3.07)	F(C=NC)	0.59	t(C—CH_3)	0.081
K(C_{lys}—R)	2.23 (3.07)	F(N—CR)	0.32	t(N—CH_2)	0.081
K(C—H)	4.83	F($HC_{lys}H$)	0.13	(6w,7w)	−0.130
K(C_{15}—H)	4.00	Non-Urey–Bradley		(8w,9CH_3w)	0.088
K(N—H)	4.83	k(C=C,C=C)	−0.280 (−0.31)	(10w,11w)	−0.063
K(C_{lys}—H)	4.71	k(C=C,C=N)	−0.700 (−0.720)	(12w,13CH_3w)	0.073
K(N—C_{lys})	2.74	k(C=C,C—C)	0.294 (−0.056)	(14w,15w)	−0.055
Chain Bends		k(C—C,C—C)	−0.051 (−0.09)	(5w,6w)	−0.172
H(CCC)	0.570 (0.57)	k(CC,CR)	0.103 (−0.14)	(7w,8w)	−0.178
H(CCC)cis[b]	0.735 (0.82)	k(CC,CC)[c]	−0.130 (−0.04)	(9CH_3w,10w)	0.174
H(C=CH)	0.300 (0.288)	m(CC,bend)[d]	0.046 (0.07)	(11w,12w)	−0.168
H(C—CH)	0.355 (0.300)	h(bend,bend)[e]	0.032 (0.06/0.04)[g]	(13CH_3w,14w)	0.172
H(RCR)	0.700 (0.75)	h(bend,bend)[f]	0.076 (0.06/0.04)[g]	(15w,Nw)	−0.138
H(CC=N)	0.570	h(CCC,CCC) trans	0.112 (0.145)	(14w,Nw)	−0.014
H(C=NC)	0.700 (0.82)	h(CCC,CCR) cis	0.338	(t,w)$_d$	0.292
H(N—CR)	0.690	CH_3 Group		(t,w)$_s$	0.116
H(N=CH)	0.191 (0.272)	K(CH)	4.709	(t(C—CH_3),w)	−0.052
H(C=NH)	0.279 (0.392)	K(C—CH_3)	2.550	l(t,CCH)	0.056
H(C—NH)	0.345 (0.329)	H(CCH)	0.395 (0.389)	l(w,CCH) methyl	0.080
H(R—CH)	0.310 (0.329)	H(HCH)	0.506	l(w,CCH) adjacent	−0.018
H(N—CH)	0.389	F(CCH)	0.480		
H($HC_{lys}H$)	0.506	F(HCH)	0.130		
H(C_6C_7H)	0.415 (0.300)	h(HCH,HCH)	−0.020		
H(C_9C_8H)	0.415 (0.300)	h(CCH,CCH)	0.034		

[a] Modified Urey–Bradley force field adapted from ref 8 and 9. Symbols used: K, diagonal stretch; H, diagonal bend; F, Urey–Bradley quadratic constant (linear term set equal to $-0.1F$); k, stretch–stretch interaction; h, bend–bend interaction (two common atoms); m, stretch–bend interaction (one common atom); t, chain torsion; (t,w)$_d$ wag–torsion interaction across double bond; (t,w)$_s$ wag–torsion interaction across single bond; (w,w) wag–wag interaction; l(t,CCH), chain torsion–methyl bend interaction; l(w,CCH), chain wag–methyl bend interaction. Stretching force constants in mdyn/Å, stretch–bend cross terms in mdyn/rad, and bending constants in mdyn Å/rad^2. PSB values are in parentheses. [b] Applies to all CCC or $CCCH_3$ bends that are cis to another such bend. [c] Applies to pairs of chain stretches separated by three or five bonds. Interactions involving the C_5=C_6 bond have not been included. [d] This term applies to all interactions between chain CC stretches and CCC or CCH bends which have a nonvertex atom of the bending angle in common. Its sign is positive if the substituents are trans and negative if they are cis. [e] Applies to bend, bend interactions across trans double bonds. [f] Applies to bend, bend interactions across trans single bonds. [g] In the *all-trans*-PSB field, all h(CCH,CCH) and h(CCC,CCH) constants were 0.06 (mdyn·Å)/rad^2, and h(CCC,CC–CH_3) constants were 0.04 (mdyn·Å)/rad^2.

1600-cm^{-1} region. The Raman spectrum of native BR_{568} (Figure 2A) exhibits only three resolved ethylenic lines at 1527, 1581, and 1600 cm^{-1}; however, peak-fitting of the intense 1527-cm^{-1} band reveals two less intense lines at 1533 and 1550 cm^{-1} (Table III). The individual stretches are significantly mixed in the normal modes due to their near degeneracy and the potential energy coupling of the C=C internal coordinates through the conjugated π-system. The relative contributions of each of the C=C stretching coordinates to the normal modes can most accurately be determined from the observed ^{13}C shifts. ^{13}C-Substitution lowers the frequency of any ethylenic normal mode which contains a component of the labeled C=C stretch. For example, a single ^{13}C-substitution in a pure C=C stretch would result in a shift of ~30 cm^{-1}. The ^{13}C data are presented in Figure 2, and the experimental and calculated frequencies are summarized in Table III.

The observed changes in intensity of the C=C vibrations upon isotopic substitution are also of interest because they provide qualitative information about the sign of each C=C component in the normal mode.[8,9] In a symmetric combination of C=C stretches, the intrinsic resonance Raman intensities of the individual stretches add to give an intense band, while in an antisymmetric stretch combination the component C=C stretching intensities tend to cancel. This simple interpretation is possible because all of the double bonds are expected to lengthen upon electronic excitation, giving ground → excited state geometry changes of the same sign. With this in mind we can use the intensity changes observed in the isotopic spectra of BR_{568} to estimate qualitatively the magnitude and sign of the C=C components in an ethylenic normal mode.

We first consider the most intense ethylenic mode at 1527 cm^{-1}. This mode is assigned as a symmetric combination of the C_{13}=C_{14}, C_{11}=C_{12}, C_9=C_{10}, C_7=C_8, and C_5=C_6 stretches with a predicted frequency of 1528 cm^{-1}. The atomic displacements for this mode are presented in Figure 3A to illustrate how the carbon atoms move in-phase in the symmetric C=C combination. The approximate contributions of each of the C=C internal coordinates to this mode can be established by looking at the isotopic derivative spectra. For example, ^{13}C-substitution at C_{13} or C_{14} (F and D in Figure 2) results in a 7- or 8-cm^{-1} shift of the 1527-cm^{-1} line, indicating a substantial contribution from the C_{13}=C_{14} stretching coordinate. This mode is calculated to shift to 1523 and 1525 cm^{-1} in the 14- and 13-^{13}C derivatives, respectively, and the shifted mode has much greater C_{13}=C_{14} character (C_{13}=C_{14} coefficient = 0.15–0.16) than calculated in the native normal mode (C_{13}=C_{14} coefficient = 0.09). ^{13}C-Substitution at C_9 or C_{10} produces a 5–7-cm^{-1} shift of the 1527-cm^{-1} line, while substitution at C_{11} or C_{12} results in a 7-cm^{-1} shift. The nearly equal ^{13}C shifts in each of these derivatives indicate that the 1527-cm^{-1} line contains approximately equal contributions from the C_{13}=C_{14}, C_{11}=C_{12},

Table II. Calculated Frequencies and Assignments for Native BR_{568}

obsd	calcd[a]	description[b]
1640	1639	0.34(C=N) - 0.12(13=14) - 0.10(14—15) - 0.10(N—C) - 0.55(NH) + 0.47(15H)
1600	1606	0.31(7=8) - 0.11(5=6) - 0.12(13=14) - 0.15(8—9) - 0.66(8H) + 0.48(7H)
	1598	0.32(5=6) + 0.11(7=8) - 0.12(9=10) - 0.09(11=12) - 0.13(6—7) + 0.10(10—11) + 0.44(7H) - 0.27(11H)
1581	1580	0.27(13=14) - 0.19(5=6) - 0.12(9=10) - 0.16(14—15) - 0.56(14H)
1533	1534	0.31(9=10) - 0.14(11=12) - 0.13(13=14) - 0.09(14—15) + 0.08(12—13) - 0.09(9-CH_3) - 0.47(10H) + 0.36(12H)
1527	1528	0.28(11=12) + 0.10(7=8) + 0.09(13=14) + 0.08(9=10) + 0.09(5=6) - 0.14(10—11) - 0.17(12—13) - 0.04(14—15) + 0.65(11H) - 0.64(12H) - 0.34(10H) + 0.27(7H)
1456	1455	(19CH_3) in-plane deformation
1456	1455	(20CH_3) in-plane deformation
1448	1450	(19CH_3) out-of-plane deformation
1448	1450	(20CH_3) out-of-plane deformation
	1395	0.59(10H) - 0.54(8H) - 0.52(7H) - 0.09(9-CH_3) + 0.08(10—11) - 0.06(12—13) + 0.08(10—11)
	1382	0.49(14H) - 0.08(13-CH_3) + 0.13(12—13) + 0.07(14—15)
1378	1371	(19CH_3) symmetric deformation
1378	1364	(20CH_3) symmetric deformation
1348	1352	0.99(NH) + 0.13(12—13) + 0.06(14—15) - 0.15(13-CH_3)
1345	1337	0.74(15H) - 0.28(NH) + 0.26(14H) + 0.15(12—13) - 0.06(14—15) - 0.11(13-CH_3)
1330	1325	0.57(7H) + 0.48(8H) + 0.48(10H) + 0.38(15H) + 0.14(8—9) - 0.18(9-CH_3)
1322	1314	0.45(12H) + 0.45(11H) + 0.32(8H) - 0.26(7H) - 0.49(15H) + 0.16(8—9) - 0.13(9-CH_3)
1304	1303	0.62(7H) - 0.58(8H) + 0.37(12H) - 0.15(7=8)
1273	1277	0.81(11H) - 0.33(12H) + 0.30(10H) - 0.17(11=12) - 0.08(10—11)
1255	1255	0.77(lysine rock) - 0.07(14—15) - 0.07(12—13) + 0.38(14H) - 0.27(15H)
1248	1244	0.14(12—13) + 0.04(14—15) - 0.68(14H) + 0.47(lysine rock) - 0.37 (15H)
1214	1218	0.18(8—9) - 0.11(14—15) - 0.53(10H) - 0.49(12H) - 0.08(9-CH_3)
1201	1201	0.26(14—15) + 0.13(8—9) - 0.26(10H) + 0.28(15H)
1169	1170	0.30(10—11) - 0.08(8—9) + 0.27(11H) - 0.19(12H)
	1124	0.32(6—7)
1048	1055	0.68(20CH_3 or) + 0.43(19CH_3 or)
	1051	0.71(19CH_3 or) - 0.43(20CH_3 or)
	1047	0.32(N—C)
1022	1009	0.56(20CH_3r) - 0.51(19CH_3r)
1008	1001	0.56(19CH_3r) + 0.53(20CH_3r)

[a] All frequencies are in cm^{-1}. [b] Coefficients ($\partial S/\partial Q$) of internal coordinates S in the normal modes Q. Symbols used: H, in-plane hydrogen rock; or, out-of-plane methyl rock; r, in-plane methyl rock. Coefficients of CC stretches are $\sim 1/6^{1/2}$ of CCH rocking coefficients having comparable potential energy contributions due to their greater reduced mass.

and C_9=C_{10} stretches. The 2–3-cm^{-1} shift of the 1527-cm^{-1} line in the 7- and 8-^{13}C derivatives indicates a smaller contribution from the C_7=C_8 stretching coordinate. The large intensity of the 1527-cm^{-1} line is consistent with the assignment of this vibration as an in-phase combination of these four stretches. The calculation produces a symmetric combination of these stretches as the lowest frequency C=C mode but with unequal coefficients. The calculated C_{11}=C_{12} stretching component in the 1527 cm^{-1} mode is too large. This is reflected in the ^{13}C shifts calculated in the 12-^{13}C and 11-^{13}C derivatives which are approximately double the observed values (Table III). On the other hand, the C_9=C_{10} stretch makes too small a contribution to the calculated 1527-cm^{-1} mode. In the 9- and 10-^{13}C derivatives, the 1527-cm^{-1} line is not calculated to shift as observed; instead the 1533-cm^{-1} line which has a large coefficient for the C_9=C_{10} stretch is calculated to shift 18–21 cm^{-1} in these derivatives. Selectively lowering the C_9=C_{10} force constant increases the proportion of C_9=C_{10} character in the "1528-cm^{-1}" mode relative to the "1534-cm^{-1}" mode; however, the frequencies for these two modes are then calculated much lower than the experimental 1527- and 1533-cm^{-1} positions. The coefficients in these highly mixed modes are sensitive to the k(C=C,C=C) and k(C=C,C—C) coupling constants,[8] and fitting to frequencies and frequency shifts does not yield accurate mode descriptions in this case.

The 1533-cm^{-1} line is calculated to be an antisymmetric combination of the C_9=C_{10} and C_{11}=C_{12} stretches. The atomic displacements of this mode are depicted in Figure 3B. The 1533-cm^{-1} line is observed to shift 7–12 cm^{-1} in the 9-, 10-, 11-, and 12-^{13}C derivatives, confirming that this mode has contributions from the C_9=C_{10} and C_{11}=C_{12} stretches. The low intensity of this mode is consistent with its being an out-of-phase combination of these two internal coordinates.

The large isotopic shifts observed in the 1581-cm^{-1} mode upon ^{13}C-substitution at C_{13} and C_{14} indicate that this mode carries approximately one-third of the C_{13}=C_{14} stretch character. In the 14-^{13}C derivative, this line shifts 8 cm^{-1} to 1573 cm^{-1}, while in the 13-^{13}C derivative a 9-cm^{-1} shift to 1572 cm^{-1} is observed. The only other ^{13}C-substitutions which appear to shift this line are at C_5 and C_6 and this will be discussed below. The C_{13}=C_{14} stretch is calculated at 1580 cm^{-1} as an antisymmetric combination with the C_9=C_{10} and C_5=C_6 stretches. The calculation reproduces the shifts in the 13- and 14-^{13}C derivatives, and also in the 5- and 6-^{13}C derivatives. The intensity increase of the ~1572-cm^{-1} line in the 13- and 14-^{13}C spectra is probably due to an increase in C_{11}=C_{12} and C_9=C_{10} character in the downshifted normal mode. The contribution of these stretches to the 1572-cm^{-1} mode is calculated to increase upon ^{13}C-substitution.

Assignment of the modes containing C_7=C_8 and C_5=C_6 stretch character is more difficult since only small shifts of the native BR_{568} lines are observed in the 5-, 6-, 7-, or 8-^{13}C derivatives. In 7- and 8-^{13}C-BR_{568} the 1600-cm^{-1} line shifts down slightly in frequency (2–8 cm^{-1}) and loses intensity, while in the [5- and 6-^{13}C] derivatives the 1581-cm^{-1} line apparently shifts *up* in frequency ~6 cm^{-1}. In addition, a shoulder appears at 1563 cm^{-1}

Table III. Observed and Calculated C=C Stretches in ^{13}C-Substituted BR_{568}

native	1640[a] (8)[b]/1639[c]	1600 (4)/1606	-/1598	1581 (5)/1580	1550 (1)	1533 (4)/1534	1527 (78)/1528	
15-[^{13}C]	1623 (5)/1619	1600 (2)/1602	-/1597	1581 (4)/1576	1544 (8)	1531 (19)/1534	1526 (62)/1527	26[d]/30[e]
14-[^{13}C]	1639 (8)/1638	1599 (6)/1604	-/1597	1573 (9)/1564	1543 (14)	1530 (9)/1530	1519 (54)/1523	28/29
14,15-[^{13}C]	1622 (6)/1616	1599 (3)/1601	-/1596	1572 (11)/1562	1544 (14)	1526 (13)/1529	1517 (53)/1520	51/61
13-[^{13}C]	1639 (8)/1636	1599 (4)/1604	-/1597	1572 (1)/1568	1545 (3)	1528 (12)/1533	1520 (57)/1525	28/22
12-[^{13}C]	1640 (10)/1638	1599 (4)/1605	-/1597	1581 (8)/1580	1543 (14)	1526 (6)/1533	1520 (58)/1508	22/24
11-[^{13}C]	1639 (9)/1639	1597 (8)/1606	-/1596	1581 (4)/1579	1542 (10)	1522 (12)/1534	1520 (57)/1513	30/18
10-[^{13}C]	1640 (11)/1639	1598 (7)/1606	-/1595	1581 (1)/1577	1545 (10)	1521 (10)/1513	1520 (61)/1530	26/25
10,11-[^{13}C]	1638 (9)/1639	1593 (16)/1606	-/1594	1581 (1)/1575	1544 (4)	1520 (16)/1517	1514 (54)/1509	41/45
9-[^{13}C]	1640 (9)/1639	1600 (5)/1605	-/1596	1580 (3)/1579	1544 (14)	1526 (7)/1516	1522 (62)/1529	19/21
8-[^{13}C]	1641 (8)/1639	-/1574	1598 (1)/1598	1582 (6)/1587	1540 (3)	1532 (6)/1534	1525 (76)/1526	11/27
7-[^{13}C]	1641 (10)/1639	-/1576	1592 (2)/1600	1583 (9)/1587	1554 (10)	1531 (9)/1534	1524 (60)/1526	-2/23
6-[^{13}C]	1641 (9)/1639	1599 (4)/1605	1563 (6)/1564	1587 (4)/1587	1541 (6)	1531 (8)/1534	1526 (63)/1526	6/30
5-[^{13}C]	1641 (9)/1639	1600 (2)/1605	-/1564	1586 (2)/1587	1545 (5)	1533 (15)/1534	1527 (67)/1526	-1/30

[a] Observed frequency (cm^{-1}). [b] Raman intensity obtained by deconvolution of the 1500–1600-cm^{-1} region of the Raman spectrum. Total Raman intensity in this region was normalized to 100. [c] Calculated frequency (cm^{-1}). [d] Sum of observed frequency shifts. [e] Sum of the calculated frequency shifts.

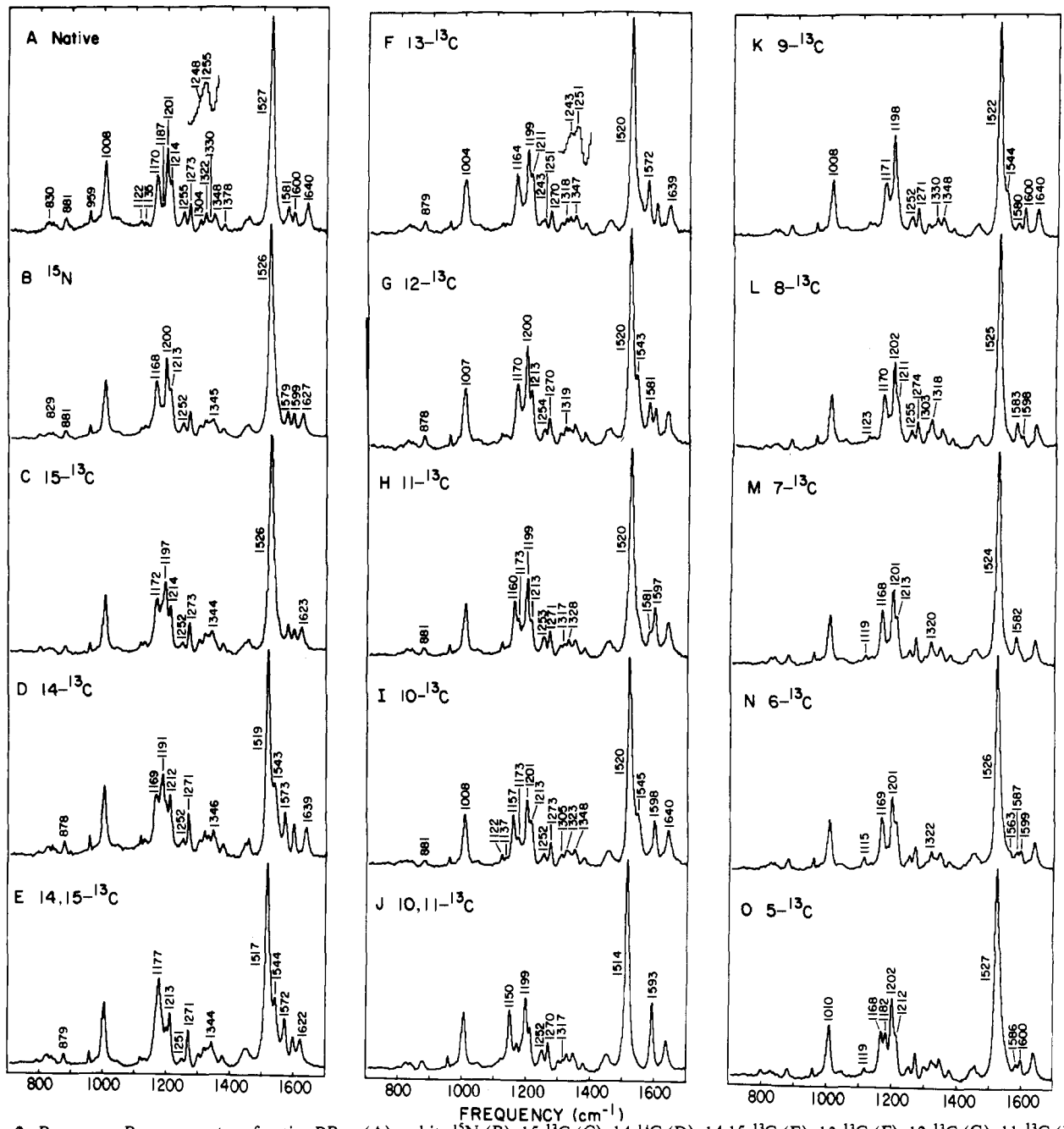

Figure 2. Resonance Raman spectra of native BR_{568} (A) and its ^{15}N (B), 15-^{13}C (C), 14-^{13}C (D), 14,15-^{13}C (E), 13-^{13}C (F), 12-^{13}C (G), 11-^{13}C (H), 10-^{13}C (I), 10,11-^{13}C (J), 9-^{13}C (K), 8-^{13}C (L), 7-^{13}C (M), 6-^{13}C (N), and 5-^{13}C (O) derivatives.

in the 6-^{13}C spectrum. The 1563-cm^{-1} line is clearly resolved in 6-^{13}C,15-D-BR_{568} (data not shown) where the intense 1527-cm^{-1} line shifts to 1522 cm^{-1}.[16] An *upshift* of the 1581-cm^{-1} mode upon ^{13}C-substitution might be expected if this line is coupled with an additional vibration which is shifted by ^{13}C-substitution from above to below 1581 cm^{-1}. The shift of the 1581-cm^{-1} line in the 5- and 6-^{13}C spectra, therefore, suggests that most of the C_5=C_6 stretch character is *above* 1581 cm^{-1} in native BR_{568} and that it shifts to ~1563 cm^{-1} in the [6-^{13}C] derivative. The C_5=C_6 and C_7=C_8 force constants were adjusted to place the C_5=C_6 and C_7=C_8 stretches at 1598 and 1606 cm^{-1}, nearly degenerate and strongly mixed, which correctly reproduces both the frequency of the C_5=C_6 stretch in the 6-^{13}C derivative (1564 cm^{-1} calculated, 1563 cm^{-1} observed) and the upshift of the 1581-cm^{-1} mode in this derivative (7 cm^{-1} calculated, 6 cm^{-1} observed). Assignment of the C_5=C_6 stretch near 1600 cm^{-1} also helps explain the apparent insensitivity of the Raman spectrum to 7- and 8-^{13}C substitution. The weak line remaining near 1600 cm^{-1} in these derivatives may be the C_5=C_6 stretching mode which appears only when the C_7=C_8 stretching mode is shifted to lower frequency. Furthermore, the sum of the ^{13}C shifts of the C=C stretches in the 5-, 6-, 7-, and 8-^{13}C derivatives (Table III) argues that the *observed* vibrational lines in the BR_{568} spectrum are insufficient to produce the ~30-cm^{-1} shift expected for a single ^{13}C-substitution so a C=C fundamental must have low intensity in the native spectrum.

In *all-trans*-retinal, both the C_7=C_8 and C_5=C_6 modes are observed and are assigned at 1611 and 1597 cm^{-1}, respectively, while in the protonated Schiff base only the C_7=C_8 stretching mode is observed at 1612 cm^{-1}. The similar frequencies of these stretches in both the 6-*s*-*cis* model compounds and 6-*s*-*trans*-BR_{568} apparently arises from a near-cancellation of the electronic and geometric effects of C_6—C_7 isomerization. In the 6-*s*-*cis* conformation, steric interactions force a 30–70° twist about the C_6—C_7 bond[24] tending to isolate the C_5=C_6 stretch electronically from the rest of the conjugated chain. The stretch–stretch interaction constants involving the C_5=C_6 stretch were therefore made much smaller than those involving the other double bond

(24) Honig, B.; Hudson, B.; Sykes, B. D.; Karplus, M. *Proc. Natl. Acad. Sci. U.S.A.* **1971**, *68*, 1289.

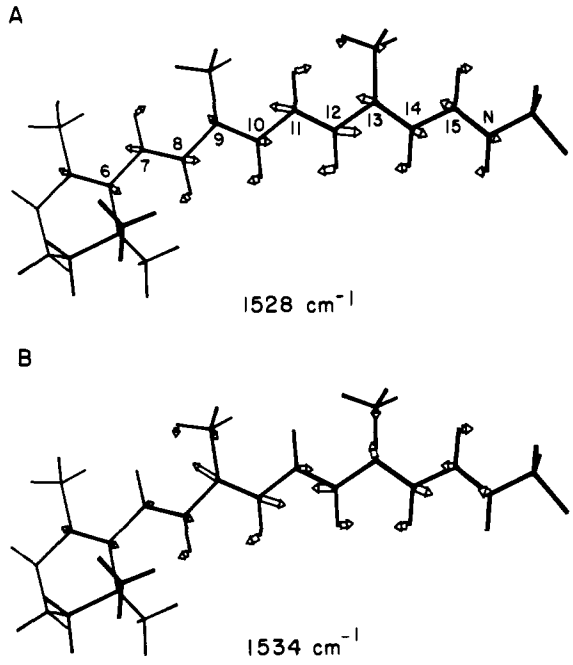

Figure 3. Mass-weighted atomic displacements for the 1528-cm^{-1} (A) and 1534-cm^{-1} (B) ethylenic stretching vibrations. The in-phase motion of the chain carbon atoms in the 1528-cm^{-1} mode produces the intense ethylenic line observed in the native BR_{568} spectrum.

Table IV. Calculated Frequencies and Assignments for *N*-D-Substituted BR_{568}

obsd	calcd	description[a]
1624	1626	0.32(C=N) - 0.13(13=14) - 0.09(14—15) + 0.47(15H) - 0.34(ND)
	1605	0.29(7=8) - 0.13(5=6) - 0.11(13=14) - 0.15(8—9) - 0.65(8H) + 0.44(7H)
1597	1597	0.31(5=6) + 0.14(7=8) - 0.11(9=10) + 0.09(11=12) - 0.14(6—7)
1577	1580	0.27(13=14) - 0.19(5=6) - 0.12(9=10) - 0.16(14—15) - 0.56(14H)
	1534	0.31(9=10) - 0.12(11=12) - 0.09(14—15) - 0.46(10H)
1528	1528	0.29(11=12) + 0.10(7=8) + 0.08(13=14) + 0.08(5=6) - 0.17(12—13) - 0.14(10—11) + 0.66(12H) - 0.65(11H)
	1393	0.63(10H) - 0.54(8H) - 0.52(7H) - 0.10(9-CH_3)
	1381	0.50(14H) - 0.07(13-CH_3)
1345	1336	0.57(15H) - 0.49(7H)
1332	1324	0.47(8H) + 0.45(7H)
1322	1313	0.41(12H) + 0.39(11H) + 0.32(8H) - 0.27(7H)
1305	1303	0.62(7H) - 0.57(8H)
1274	1277	0.82(11H) - 0.28(12H) + 0.30(10H) - 0.17(11=12)
1248	1262	0.12(12—13) + 0.10(14—15) - 0.63(14H) - 0.06(13-CH_3)
1253	1249	0.82(lysine rock) - 0.43(15H)
1214	1218	0.18(8—9) + 0.08(12—13) - 0.12(14—15) - 0.08(9-CH_3)
1201	1204	0.24(14—15) + 0.15(8—9)
1171	1170	0.30(10—11) - 0.08(8—9)
	1124	0.32(6—7)
977	974	0.63(ND)

[a] See footnotes to Table II.

stretches in the retinal and PSB force fields. If the same stretch–stretch interaction constants are transferred to the 6-*s*-*trans* geometry, the altered kinetic coupling through the *s*-*trans* bond causes the C_5=C_6 and C_7=C_8 stretches to couple strongly and split far apart in frequency. However, there is probably little twist about the C_6—C_7 bond in the 6-*s*-*trans* conformer, so the C_5=C_6 stretch should be more fully conjugated with the rest of the chain, and the interaction constants involving this stretch should be similar to those for the other double bond stretches. When these changes in the force field are made, the C_5=C_6 and C_7=C_8 stretches become only weakly coupled and nearly degenerate in

Table V. Calculated Frequencies and Assignments for 15-D-Substituted BR_{568}

obsd	calcd	description[a]
1629	1632	0.32(C=N) - 0.16(13=14) - 0.10(N—C) - 0.56(NH)
	1604	0.31(7=8) - 0.13(5=6) - 0.07(13=14) - 0.15(8—9) - 0.67(8H)
1601	1598	0.32(5=6) + 0.12(7=8) - 0.11(9=10) + 0.44(7H)
1580	1575	0.26(13=14) - 0.18(5=6) - 0.15(9=10) - 0.17(14—15) - 0.55(14H)
	1533	0.26(9=10) - 0.22(11=12) - 0.47(10H)
1522	1526	0.22(11=12) + 0.17(9=10) + 0.15(13=14) + 0.09(5=6) + 0.60(11H)
	1394	0.62(10H) - 0.55(8H) - 0.55(7H)
	1382	0.53(14H) - 0.08(13-CH_3)
1349	1345	0.98(NH) + 0.15(12—13)
1332	1327	0.64(7H) + 0.42(8H) + 0.47(14H)
1323	1319	0.45(12H) + 0.36(11H) + 0.37(8H) + 0.21(8—9)
1304	1303	0.66(7H) - 0.61(8H)
1271	1277	0.82(11H) - 0.31(12H)
1271	1271	0.83(lysine rock) - 0.13(14—15)
	1248	0.17(12—13) + 0.02(14—15) - 0.74(14H) - 0.05(13-CH_3)
1215	1220	0.16(14—15) - 0.15(8—9) + 0.06(9-CH_3)
1215	1208	0.17(8—9) + 0.19(14—15) - 0.08(9-CH_3)
1171	1170	0.30(10—11)
	1124	0.31(6—7)
974	981	0.76(15D)

[a] See footnotes to Table II.

Table VI. Calculated Frequencies and Assignments for 14-D-Substituted BR_{568}

obsd	calcd	description[a]
1636	1639	0.34(C=N) - 0.13(13=14) - 0.10(N—C) - 0.56(NH) + 0.47(15H)
	1604	0.33(7=8) - 0.09(5=6) - 0.11(13=14) - 0.15(8—9)
1598	1597	0.35(5=6) + 0.07(7=8) - 0.12(9=10) - 0.13(6—7)
1574	1568	0.26(13=14) - 0.20(9=10) - 0.16(5=6)
	1530	0.31(11=12) - 0.12(9=10) - 0.17(12—13) + 0.54(11H)
1521	1524	0.25(9=10) + 0.23(13=14) - 0.30(10H)
	1393	0.66(10H) - 0.56(8H) - 0.56(7H)
1348	1354	1.1(NH) + 0.49(15H) + 0.05(12—13)
	1347	0.49(15H) - 0.51(NH) - 0.10(12—13)
1317	1331	0.20(12—13) - 0.45(NH) - 0.15(13-CH_3)
	1322	0.45 (7H) + 0.40(8H) + 0.46(10H)
1307	1314	0.49(12H) + 0.47(11H) - 0.30(7H) - 0.31(8H)
1297	1302	0.60(7H) - 0.59(8H)
1272	1275	0.76(11H) - 0.45(12H)
	1251	0.92(lysine rock) + 0.01(12—13) - 0.02(14—15)
1216	1217	0.22(8—9) - 0.07(9-CH_3)
1193	1195	0.26(14—15)
1174	1171	0.30(10—11) - 0.09(8—9)
	1124	0.32(6—7)
972/984	973	0.60(14D)

[a] See footnotes to Table II.

frequency, consistent with the experimental observations.

Finally, assignment of the C_5=C_6 and C_7=C_8 stretching modes near 1600 cm^{-1} implies that the vibrational line observed at 1550 cm^{-1} is not a fundamental.[25] Our only reservation with this assignment is that this mode is observed with moderate intensity at 1544 cm^{-1} in the 11,12-D_2-BR_{568} spectrum (Figure 4H). Since combination bands are expected to be weak in the Raman spectrum, the intensity of the 1544-cm^{-1} line must result from a combination of an intense mode between ~1000 and 1500 cm^{-1} and a much weaker mode below ~600 cm^{-1}, or from mixing with nearby fundamentals.

(25) To verify that the 1550-cm^{-1} line does not arise from photolysis of the BR_{568} pigment, spectra were obtained of the 12,20-D_4 derivative (in which the 1550-cm^{-1} mode is clearly resolved) with the photoalteration parameter (*F*) ranging from 0.01 to 0.3. No changes in relative intensity were observed. We also note that in the 14-[^{13}C] derivative of *all*-*trans*-retinal,[29] a band is observed at 1552 cm^{-1} which is assigned as a combination band.

Table VII. Calculated Frequencies and Assignments for 12-D-Substituted BR_{568}

obsd	calcd	description[a]
1638	1638	0.35(C=N) - 0.12(13=14) - 0.10(N—C) - 0.56(NH) + 0.48(15H)
	1605	0.31(7=8) - 0.12(5=6) - 0.12(13=14) - 0.15(8—9)
1598	1598	0.32(5=6) + 0.13(7=8) - 0.15(9=10) - 0.13(6—7)
1580	1579	0.28(13=14) - 0.19(5=6) - 0.11(9=10) - 0.56(14H)
	1533	0.32(9=10) + 0.15(13=14) - 0.11(10—11) - 0.46(10H)
1513	1510	0.32(11=12) + 0.09(7=8) - 0.20(12—13) + 0.68(11H)
	1388	0.65(10H) - 0.13(12—13) - 0.09(9-CH_3) - 0.50(8H)
	1378	0.49(14H) - 0.08(13-CH_3)
1348	1348	0.81(NH) + 0.11(12—13)
	1334	0.82(15H) + 0.16(12—13)
1328	1322	0.50(7H) + 0.47(8H) + 0.55(10H)
1305	1308	0.68(7H) - 0.53(8H)
1274	1291	0.79(11H) + 0.13(12—13)
1254	1257	0.57(lysine rock) + 0.08(12—13) + 0.05(14—15) + 0.05(10—11) + 0.02(8—9) + 0.48(14H)
1244	1250	0.06(12—13) + 0.07(8—9) + 0.07(10—11)
1224	1234	0.11(8—9) + 0.10(10—11) - 0.13(14—15) - 0.04(12—13)
1198	1199	0.25(14—15) + 0.15(8—9)
1183	1176	0.29(10—11) - 0.11(8—9)
	1124	0.32(6—7)
980	979	0.53(12D)

[a] See footnotes to Table II.

Table VIII. Calculated Frequencies and Assignments for 11-D-Substituted BR_{568}

obsd	calcd	description[a]
1638	1639	0.35(C=N) - 0.13(13=14) - 0.10(N—C) - 0.56(NH) + 0.47(15H)
	1606	0.31(7=8) - 0.11(5=6) - 0.12(13=14) - 0.16(8—9)
1596	1596	0.34(5=6) + 0.12(7=8) - 0.12(9=10) - 0.13(6—7)
1583	1578	0.28(13=14) - 0.14(5=6) - 0.12(9=10) - 0.56(14H)
	1534	0.31(9=10) + 0.18(13=14) - 0.13(11=12) - 0.49(10H)
1515	1511	0.30(11=12) + 0.11(9=10) + 0.07(5=6) + 0.07(7=8) - 0.67(12H)
	1390	0.71(10H) - 0.50(8H) - 0.47(7H)
	1381	0.52(14H) - 0.08(13-CH_3)
1348	1351	0.99(NH) + 0.13(12—13)
	1334	0.90(15H) + 0.14(12—13)
1328	1324	0.54(7H) + 0.52(8H) + 0.56(10H)
1319	1306	0.70(7H) - 0.56(8H)
1302	1293	0.70(12H)
1254	1255	0.78(lysine rock) - 0.07(14—15) - 0.06(12—13)
	1244	0.14(12—13) + 0.67(14H) - 0.06(13-CH_3)
1209	1219	0.19(8—9) - 0.13(14—15) + 0.08(12—13) - 0.08(9-CH_3)
1201	1200	0.26(14—15) + 0.13(8—9) + 0.06(10—11)
1171	1186	0.30(10—11)
	1124	0.32(6—7)
960	974	0.60(11D)

[a] See footnotes to Table II.

The normal mode character of the C=C stretches indicated by the ^{13}C shifts is supported by shifts observed in the deuterium derivatives. The deuterium data are presented in Figure 4, and the normal mode frequencies are summarized in Tables IV–X. Kinetic coupling of the C=C stretches with the CCH rocks produces normal modes which contain both C=C stretch and CCH rock character. Deuteriation removes the coupling between the C=C stretches and CCH rocks by lowering the frequency of the deuteriated rock from 1300–1400 cm^{-1} to ~980 cm^{-1}.

The 1527-cm^{-1} line shifts to lower frequency upon deuteriation at positions 14, 12, 11, 10, 8, and 7 when coupling of the CCH rocks with the associated C_{13}=C_{14}, C_{11}=C_{12}, C_9=C_{10}, and C_7=C_8 stretches is removed. Deuteriation is such a large perturbation that it changes the character of the normal modes; the general trend is to increase the character of the deuteriated C=C stretch in the downshifted mode while pushing the contribution of the other stretching coordinates into the higher frequency C=C

Table IX. Calculated Frequencies and Assignments for 10-D-Substituted BR_{568}

obsd	calcd	description[a]
1641	1639	0.35(C=N) - 0.13(13=14) - 0.10(N—C) - 0.56(NH) + 0.47(15H)
	1606	0.31(7=8) - 0.11(5=6) - 0.12(13=14) - 0.67(8H)
1597	1595	0.35(5=6) + 0.11(7=8) - 0.13(6—7) + 0.44(7H)
1581	1577	0.30(13=14) - 0.12(5=6) - 0.17(14—15)
1526	1531	0.29(11=12) - 0.16(9=10) + 0.59(11H) - 0.62(12H)
1520	1515	0.31(9=10) + 0.12(11=12) + 0.11(13=14)
	1385	0.61(14H) - 0.08(13-CH_3)
	1359	0.65(7H) + 0.56(8H)
1348	1352	0.99(NH) + 0.12(12—13)
	1337	0.62(15H) + 0.29(NH)
1321	1316	0.61(12H) + 0.58(11H)
	1306	0.70(8H) - 0.45(7H) - 0.11(8—9)
1294	1292	0.22(8—9) + 0.40(7H) - 0.17(8H)
1272	1269	0.62(11H) - 0.27(12H) + 0.13(8—9)
	1252	0.83(lysine rock) - 0.07(14—15) - 0.03(12—13)
1237	1240	0.13(12—13) + 0.10(14—15) - 0.73(14H)
1204	1204	0.28(14—15)
1165	1167	0.28(10—11)
	1124	0.32(6—7)
972	970	0.53(10D)

[a] See footnotes to Table II.

Table X. Calculated Frequencies and Assignments for 8-D-Substituted BR_{568}

obsd	calcd	description[a]
1640	1639	0.36(C=N) - 0.12(13=14) - 0.56(NH) + 0.47(15H)
1595	1598	0.33(5=6) - 0.13(9=10)
	1589	0.26(7=8) - 0.22(13=14)
1580	1577	0.21(7=8) + 0.19(13=14)
	1532	0.25(9=10) - 0.24(11=12)
1519	1525	0.20(9=10) + 0.19(11=12) + 0.14(7=8) + 0.13(13=14)
	1386	0.58(14H) + 0.27(10H)
	1378	0.46(10H)
1346	1350	1.07(NH)
	1335	0.84(15H) + 0.13(12—13)
1316	1317	0.97(7H) + 0.11(8—9)
	1311	0.56(12H) + 0.51(11H) + 0.17(8—9)
1275	1277	0.79(11H) - 0.35(12H)
1253	1255	0.75(lysine rock) - 0.08(14—15) - 0.07(12—13)
	1245	0.13(12—13) + 0.04(14—15) - 0.07(8—9)
1223	1227	0.21(8—9) + 0.07(12—13) - 0.09(9-CH_3)
1202	1204	0.27(14—15) + 0.08(8—9)
1169	1174	0.29(10—11) - 0.04(8—9)
	1125	0.33(6—7)
980	986	0.35(8D)

[a] See footnotes to Table II.

fundamentals. In 14D BR_{568}, the 1527-cm^{-1} line shifts 6 cm^{-1} (4 cm^{-1} calculated) to 1521 cm^{-1}, reflecting the C_{13}=C_{14} stretch character in the 1527-cm^{-1} vibration. The shifted C=C mode is calculated as a symmetric combination of the C_{13}=C_{14} and C_9=C_{10} stretches with a large increase in the C_{13}=C_{14} coefficient (Table VI). C_{11}=C_{12} stretch character is predicted to shift into the 1530-cm^{-1} mode. Deuteriation at C_{12} shifts the 1527-cm^{-1} mode to 1513 cm^{-1} (1510 cm^{-1} calculated). This mode is predicted to be a symmetric combination of the C_{11}=C_{12} and C_7=C_8 stretches. C_{11}=C_{12} character is calculated to increase in the 1510-cm^{-1} mode, while C_{13}=C_{14} character shifts into the 1533-cm^{-1} mode. Similar shifts are observed and calculated for the 11D derivative, confirming the contribution of C_{11}=C_{12} stretch character in the 1527-cm^{-1} vibration. Deuteriation of both the 11 and 12 positions produces a low-frequency mode at 1491 cm^{-1} which is calculated to be a nearly isolated C_{11}=C_{12} stretch (results not shown). Significant intensity in this mode argues that the C_{11}=C_{12} coordinate carries much of the intrinsic Raman intensity in BR_{568}. Deuteriation at C_{10} shifts the 1527-cm^{-1} line to 1520 cm^{-1} (1515 cm^{-1} calculated), while deuteriation at C_8 shifts the 1527-cm^{-1} mode to 1519 cm^{-1} (1525 cm^{-1} calculated). These shifts confirm the contribution from the C_9=C_{10} and C_7=C_8 stretches, respectively. Finally, the 1527-cm^{-1} line shifts 5 cm^{-1} in 15-D-

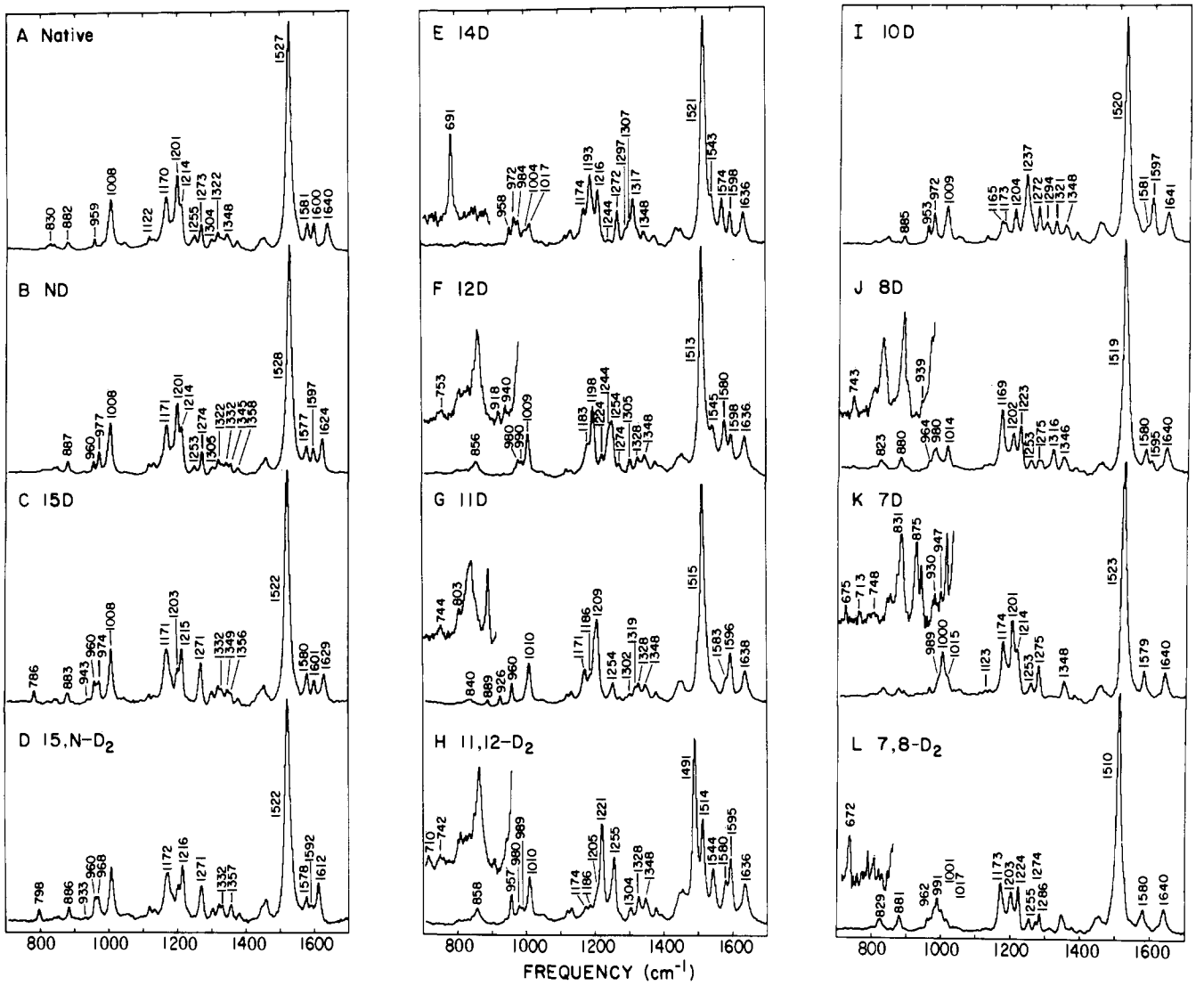

Figure 4. Resonance Raman spectra of native BR_{568} (A) and its *N*-D (B), 15-D (C), 15,*N*-D_2 (D), 14-D (E), 12-D (F), 11-D (G), 11,12-D_2 (H), 10-D (I), 8-D (J), 7-D (K), and 7,8-D_2 (L) derivatives.

BR_{568}, indicating that the $C_{15}H$ rock is weakly coupled with this mode.

The 1533-cm^{-1} line shifts to 1514 cm^{-1} in 11,12-D_2-BR_{568}, the only derivative in which this line is clearly resolved. The 1533-cm^{-1} mode is calculated to shift only 4 cm^{-1} in this derivative, arguing that the predicted $C_{11}=C_{12}$ contribution to the mode is too low.

In 7-D-, 8-D-, and 7,8-D_2-BR_{568}, the 1600-cm^{-1} line loses intensity and only a weak shoulder is observed at ~1595 cm^{-1} corresponding to the $C_5=C_6$ stretching vibration. The 1598-cm^{-1} $C_5=C_6$ stretch is calculated to shift only slightly in these derivatives, whereas the 1606-cm^{-1} $C_7=C_8$ stretch is calculated to shift more than 10 cm^{-1}. These shifts support the assignments derived from the ^{13}C derivatives.

C=N Stretch. The 1640-cm^{-1} Schiff base mode is expected to be strongly coupled with the NH and $C_{15}H$ rocks.[26] The 16-cm^{-1} shift of the 1640-cm^{-1} line to 1624 cm^{-1} in ND BR_{568} was first used to assign this line as the C=N stretching vibration.[27] A 11-cm^{-1} shift of the 1640-cm^{-1} line in 15-D-BR_{568} subsequently demonstrated the $C_{15}H$ rock contribution.[17] Our ND and 15D spectra (Figure 4, B and C) are in agreement with these results. The C=N stretching component of the Schiff base mode is evident from the 17-cm^{-1} shift when C_{15} is labeled with ^{13}C (Figure 2C)

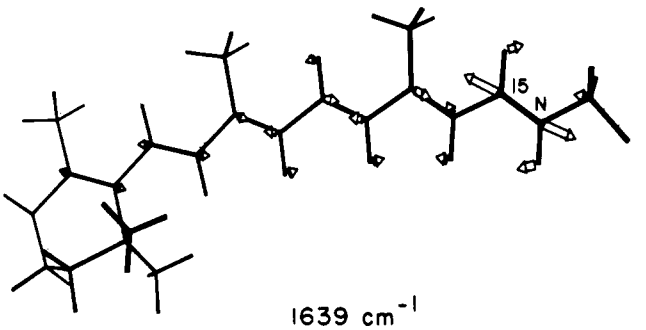

Figure 5. Mass-weighted atomic displacements for the Schiff base stretching mode.

and the 13-cm^{-1} shift when the Schiff base nitrogen is labeled with ^{15}N (Figure 2B).[28] Refinement of the force field for the Schiff base moiety requires explicit consideration of the NH and $C_{15}H$ rocking coordinates since they contribute significantly to the Schiff base mode. Thus, it is first necessary to adjust the diagonal rocking force constants in order to place the NH and $C_{15}H$ rocking modes at their observed frequencies (1348 and 1345 cm^{-1}, see below). The 1640-cm^{-1} frequency and the $^{13}C_{15}$, ^{15}N, *N*-D, and 15-D shifts

(26) Aton, B.; Doukas, A. G.; Narva, D.; Callender, R. H.; Dinur, U.; Honig, B. *Biophys. J.* **1980**, *29*, 79.

(27) Lewis, A.; Spoonhower, J.; Bogomolni, R. A.; Lozier, R. H.; Stoeckenius, W. *Proc. Natl. Acad. Sci. U.S.A.* **1974**, *71*, 4462.

(28) Argade, P. V.; Rothschild, K. J.; Kawamoto, A. H.; Herzfeld, J.; Herlihy, W. C. *Proc. Natl. Acad. Sci. U.S.A.* **1981**, *78*, 1643.

Table XI. ^{13}C Shifts of the C–C Stretches in BR_{568}[a]

	C_{10}–C_{11}	C_{14}–C_{15}	C_8–C_9	C_{12}–C_{13}	
native	1169 (1170)	1201 (1201)	1214 (1218)	1248 (1244)	1255 (1255)
15-^{13}C	−1 (−1)	−4 (−12)	0 (−1)	−2 (−2)	−2 (−1)
14	−3 (−1)	−10 (−14)	−1 (−2)	−2 (0)	−3 (−1)
14,15	−2 (−3)	−24 (−26)	−1 (−2)	−2 (−2)	−3 (−2)
13	−5 (−1)	−2 (−2)	−2 (−1)	−5 (−7)	−3 (−1)
12	0 (0)	−1 (−2)	−1 (0)	−1 (−2)	−1 (0)
11	−9 (−14)	−2 (−2)	0 (−1)	−1 (−1)	−2 (−1)
10	−12 (−15)	0 (−1)	0 (0)	−3 (0)	−2 (0)
10,11	−19 (−28)	−2 (−2)	−1 (−1)	−1 (−1)	−2 (−1)
9	−3 (−4)	−3 (−8)	−16 (−7)	−2 (−1)	−2 (0)
8	0 (−1)	0 (−2)	−3 (−2)	0 (0)	0 (0)
7	0 (−1)	0 (0)	0 (0)	− (0)	0 (0)
6	−1 (−1)	0 (0)	0 (0)	−1 (0)	0 (0)

[a] Calculated ^{13}C shifts are in parentheses. All frequencies are in wavenumbers.

are then reproduced by adjusting the C=N stretching force constant, as well as the rock–stretch interaction and Urey–Bradley constants. The calculated normal mode has large $C_{15}H$ and NH rocking coefficients (Table II) as illustrated by the atomic displacements for the Schiff base mode in Figure 5. The C=N stretch is very weakly mixed with the lower frequency C=C stretches as demonstrated by the ≤2-cm^{-1} shift of the 1640-cm^{-1} frequency upon ^{13}C-substitution of the skeletal carbons other than on the C=N moiety. In addition, ^{13}C=N or C=^{15}N substitution does not produce shifts of more than 2–3 cm^{-1} in the observed ethylenic modes.

C—C Stretches. The normal mode character of the C–C stretching modes can be determined by specific labeling with ^{13}C and ^{2}H. The observed ^{13}C shifts reveal the contributions of the individual C–C stretching internal coordinates to each normal mode, while deuterium derivatives establish the extent of coupling of the C–C stretching coordinates with the CCH in-plane rocks. The C–C stretches are strongly coupled with the CCH rocks, resulting in normal modes which are highly mixed combinations of these two sets of internal coordinates. This stretch–rock coupling is manifested by the large upshift of the stretching vibrations when coupling with the rocks is removed by deuteriation. Nevertheless, it is useful to discuss these modes as "C–C stretches" both for convenience and because the C–C internal coordinate character is often localized and can be accurately determined by ^{13}C-substitution. In addition when the normal mode coefficients are examined it is important to note that the coefficients of the C–C internal coordinates are $\sim 1/6^{1/2}$ of the CCH rock coefficients having comparable potential energy contributions because of their different reduced mass. A summary of the observed ^{13}C shifts of the C–C stretching modes is presented in Table XI.

C_{14}–C_{15} stretch character is found at 1201 cm^{-1} on the basis of a 4-cm^{-1} shift of this mode in 15-^{13}C-BR_{568}, a 10-cm^{-1} shift in 14-^{13}C-BR_{568}, and a 24-cm^{-1} shift in the 14,15-^{13}C derivative. The insensitivity of the 1169-, 1214-, 1248-, and 1255-cm^{-1} modes to ^{13}C-substitution at positions 14 and 15 indicates that in the 1170–1255-cm^{-1} C–C stretch region, C_{14}–C_{15} stretch character is found predominantly in the 1201-cm^{-1} mode. Of course, C_{14}–C_{15} stretching character is also associated with normal modes involving the C=N and C_{13}=C_{14} stretches, as well as the NH and $C_{15}H$ rocks (see Table II), so that the distribution of C_{14}–C_{15} stretch character among all the normal modes of the molecule is complicated. However, if we focus on the distribution of C_{14}–C_{15} character in the skeletal C–C stretching modes, Table XI clearly shows that this coordinate is "localized" at 1201 cm^{-1}. The C_{14}–C_{15} stretch is calculated at 1201 cm^{-1} as a symmetric combination of the C_{14}–C_{15} and C_8–C_9 stretches. The shifts of this mode in the various 14-^{13}C and 15-^{13}C derivatives are in good agreement with the calculated shifts (Table XI).

The C_{10}–C_{11} stretch is assigned at 1169 cm^{-1} on the basis of a 9-cm^{-1} shift in 11-^{13}C-BR_{568}, a 12-cm^{-1} shift in 10-^{13}C-BR_{568}, and a 19-cm^{-1} shift in the 10,11-^{13}C derivative. Since the 1201-, 1214-, 1248-, and 1255-cm^{-1} modes shift less than 4 cm^{-1} in these derivatives, it is clear that C_{10}–C_{11} stretch character is quite localized at 1169 cm^{-1}. The calculated shift for the 10,11-^{13}C derivative (28 cm^{-1}) is significantly larger than the observed shift of 19 cm^{-1}. This discrepancy arises because the downshifted $^{13}C_{10}$–$^{13}C_{11}$ stretch couples with the 1122- and 1134-cm^{-1} ionone ring modes and cannot express its full ^{13}C shift. Identical behavior has been observed and explained in the *all-trans*-PSB.[9] Thus, this frequency error arises because the cyclohexene ring was not included in the calculation.

The C_8–C_9 stretch, assigned at 1214 cm^{-1}, shifts ~16 cm^{-1} in the 9-^{13}C derivative and 3 cm^{-1} when C_8 is labeled. The difference in sensitivity of the 1214-cm^{-1} line to ^{13}C-substitution at C_8 and C_9 originates from the reduced motion of C_8 in this normal mode. This results from coupling of the C_8–C_9 stretch with the C_9–CH_3 stretch and the $C_{10}H$ rock as has been discussed in detail for *all-trans*-retinal[8] and the *all-trans*-PSB.[9]

The C_{12}–C_{13} stretch character is more delocalized so it is not possible to assign an individual normal mode as a localized C_{12}–C_{13} stretch. 13-^{13}C-Substitution results in a 5-cm^{-1} shift of the 1169-cm^{-1} line, a 5-cm^{-1} shift of a line at 1248 cm^{-1}, and 2–3-cm^{-1} shifts of the 1201-, 1214-, and 1255-cm^{-1} lines. Similar behavior has been observed in *all-trans*-retinal and the *all-trans*-PSB. In the PSB, the C_{12}–C_{13} stretching coordinate makes a large contribution to the 1237-cm^{-1} mode, consistent with its assignment as the highest frequency C–C stretch in *all-trans*-retinal (1216 cm^{-1}). In bacteriorhodopsin, increased π-electron delocalization results in an upshift of the C_{10}–C_{11}, C_8–C_9, and C_{14}–C_{15} stretches by ~10 cm^{-1} relative to the PSB.[9] A similar shift of the "C_{12}–C_{13} stretch" in BR_{568} would lead to an assignment at ~1247 cm^{-1}. In the native BR_{568} spectrum there are two lines near this frequency at 1248 and 1255 cm^{-1}. Both lines are slightly sensitive to ^{13}C-substitution at nearly all positions along the retinal chain (Table XI). However, the 1248-cm^{-1} line clearly shifts away (5 cm^{-1}) from the more intense 1255-cm^{-1} line only in the 13-^{13}C derivative (Figure 2F, inset). Thus, we assign the 1248-cm^{-1} line as the "C_{12}–C_{13} stretch", although the C_{12}–C_{13} stretching coordinate is mixed with the 1255-cm^{-1} mode as a result of its near degeneracy and also contributes to the 1169-cm^{-1} mode. The assignment of the 1255-cm^{-1} mode will be discussed below. Initial calculations on BR_{568} were unable to reproduce the 1248-cm^{-1} frequency of the "C_{12}–C_{13} stretch". Increasing the C_{12}–C_{13} stretching constant acted mainly to drive stretching character out of the normal mode without significantly raising its frequency. To raise the C_{12}–C_{13} frequency in the BR_{568} calculation, we have increased the C_{12}–C_{13} stretching constant as well as the C—CH and C=CH bending constants, thereby influencing both the stretching and rocking components in the mode. The C_{12}–C_{13} stretch is calculated at 1244 cm^{-1} with large contributions from the $C_{14}H$ and lysine CH_2 rocking coordinates. The vibrational calculation is able to reproduce the shifts observed in the 1170–1250-cm^{-1} region of the 13-^{13}C-BR_{568} spectrum with the exception of the 5-cm^{-1} shift observed in the 1169-cm^{-1} mode (1 cm^{-1} calculated).

Assignment of the C_6–C_7 stretch in BR_{568} is facilitated by comparison with *all-trans*-retinal. In ATR the C_6–C_7 stretch is at 1174 cm^{-1} and it shifts 4 cm^{-1} in the 6-^{13}C and 2 cm^{-1} in the 7-^{13}C derivative.[29] The small shifts observed in ATR apparently

result from coupling of the C_6–C_7 stretch with the stretching vibrations of the cyclohexene ring which serves to distribute C_6–C_7 stretch character into a number of normal modes. This is consistent with the observation that the 1174-cm^{-1} line in ATR is sensitive to modifications at C_5 of the cyclohexene ring such as demethylation.[29] In BR_{568}, a line is observed at 1174 cm^{-1} (clearly resolved at 1173 cm^{-1} in the 10,11-^{13}C spectrum, Figure 2J). However, this mode does not shift in the 6- or 7-^{13}C derivatives (as determined by peak fitting). The fingerprint line which is most sensitive to ^{13}C-substitution at C_6 and C_7 is the 1122-cm^{-1} mode. This line shifts 7 cm^{-1} in the 6-^{13}C derivative and 3 cm^{-1} in the 7-^{13}C derivative. A weak line at this frequency is observed in both ATR and β-ionone where it is assigned as a vibration of the cyclohexene ring. Thus, we are tentatively assigning the "C_6–C_7 stretch" at 1122 cm^{-1}, although it appears likely that the C_6–C_7 stretch is not localized, but rather contributes to a number of modes. This assignment is supported by QCFF calculations on β-ionone. In 6-*s-cis*-β-ionone, the C_6–C_7 stretch is localized in a mode at 1175 cm^{-1} and contributes to a ring mode (the *gem* methyl rock) at 1140 cm^{-1}. In the 6-*s-trans* geometry, the C_6–C_7 character splits into a mode at 1203 cm^{-1} in combination with the C_1–C_6 stretch and a mode at 1168 cm^{-1}, which has contributions from the C_4–C_5 stretch. The contribution of C_6–C_7 character to the ring mode at 1140 cm^{-1} also *increases* in the 6-*s-trans* geometry. This suggests that the sensitivity of the 1122-cm^{-1} ring mode to $^{13}C_6$- and $^{13}C_7$-substitution in BR_{568} may be a direct result of the 6-*s-trans* structure.

Vibrational analysis of the deuterium shifts of the C–C stretching modes is important for understanding the interactions between the in-plane hydrogen rocks and the C–C stretches, and it also aids in the normal mode assignments. We begin by noting that the C–C stretching region of BR_{568} is insensitive to deuteriation of the Schiff base nitrogen (Figure 4B, Table IV). In particular, no change is observed in the frequency of the 1201-cm^{-1} C_{14}–C_{15} stretching mode. We argued previously that N-deuteriation would not significantly shift the C_{14}–C_{15} frequency if the C=N bond were in the trans (or anti) configuration.[22a] The present calculation where the entire retinal chromophore is considered similarly predicts a small (3 cm^{-1}) ND induced shift of the C_{14}–C_{15} stretching mode for the C_{15}=N anti geometry.

In contrast to the ND spectrum, deuteriation at C_{15} has pronounced effects on the C–C stretches (Figure 4C, Table V). 15-D substitution results in increased intensity at 1215 and 1271 cm^{-1} and loss of intensity at 1201 and 1255 cm^{-1}. An increase of intensity at 1215 cm^{-1} is in agreement with a calculated shift of the C_{14}–C_{15} stretch from 1201 to 1220 cm^{-1}. To account for intensity loss at 1255 cm^{-1} and increased intensity at 1271 cm^{-1}, it is necessary to examine other vibrations which may be affected by 15-deuteriation. In the *all-trans*-PSB, 15-deuteriation resulted in loss of intensity in the 1237-cm^{-1} "C_{12}–C_{13} stretch" due to a drop in the contribution of the C_{14}–C_{15} stretching coordinate to the normal mode.[9] In BR_{568}, an analogous loss of C_{14}–C_{15} character may explain the loss of intensity of the weak 1248-cm^{-1} shoulder. However, the 15-D-induced shifts in bacteriorhodopsin appear more complicated; two additional vibrations at 1255 and 1271 cm^{-1} undergo changes in intensity. The initial explanation for the loss of intensity at 1255 cm^{-1} was the assignment of this vibration as the $C_{15}H$ in-plane rock.[30] However, this can be excluded on the basis of the clear assignment of the $C_{15}H$ rock at 1345 cm^{-1} (see CCH rocks below). Alternatively, the 1255-cm^{-1} mode may be assigned to an in-plane rocking vibration of the methylene protons attached to the ϵ-carbon of lysine. This mode is calculated at 1255 cm^{-1} (see Table II) with significant contributions from the C_{14}–C_{15} stretch and the $C_{15}H$ rock, and it is predicted to shift to 1271 cm^{-1} upon 15-deuteriation. The lysine–CH_2 rock is found at 1311 cm^{-1} in QCFF-π calculations on the *all-trans*-PSB, indicating that its assignment at 1255 cm^{-1} in BR_{568} is reasonable. Additional support for this assignment comes from Raman spectra of the CD_2 derivative of the *all-trans*-PSB.[16] Although the ϵ-CH_2 vibration is not observed in the PSB spectrum, the 1345-cm^{-1} $C_{15}H$ rock drops 6 cm^{-1} and gains intensity in the CD_2 PSB spectrum. The downshift of this mode indicates that the lysine–CH_2 and $C_{15}H$ rocks are coupled and that the lysine–CH_2 rocking mode is below 1345 cm^{-1}. One other normal mode which may be present at ~1255 cm^{-1} is a cyclohexene ring vibration which is observed as an intense Raman line at 1254 cm^{-1} in β-ionone and as a weak line in *all-trans*-retinal[8] and its unprotonated and protonated Schiff bases.[9] However, since this line would not be expected to be influenced by deuteriation at the Schiff base, we are assigning the 1255-cm^{-1} mode in BR_{568} as the in-plane rock of the lysine–CH_2 group.

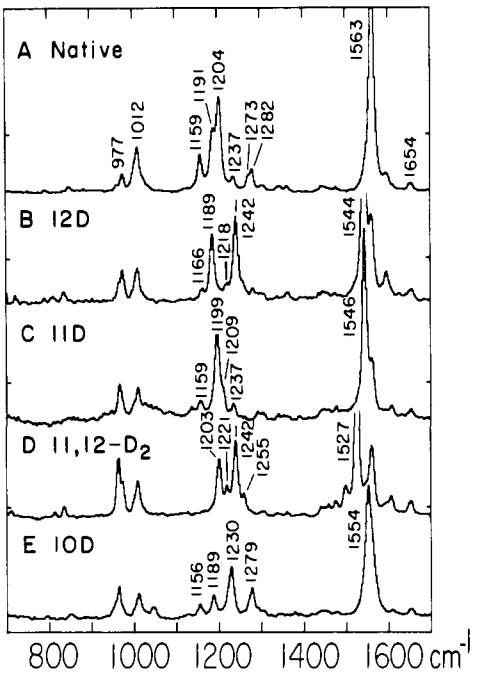

Figure 6. Raman spectra of the *all-trans*-retinal protonated Schiff base (A) and its 12-D (B), 11-D (C), 11,12-D_2 (D), and 10-D (E) derivatives.

The spectrum of 14-D-BR_{568} is shown in Figure 4E and the calculated normal modes are presented in Table VI. Previous studies of retinals have shown that the $C_{14}H$ rock is strongly coupled with the C_{12}–C_{13} stretch.[29] Deuteriation at C_{14} removes the rock–stretch coupling and in ATR results in an 83-cm^{-1} upshift of C_{12}–C_{13} stretching character. The C_{14}–C_{15} stretch characteristically drops 6 cm^{-1} in the 14-D ATR derivative. In the 14-D-BR_{568} spectrum the intensity loss at 1248- and 1255-cm^{-1} lines probably results from an upshift of C_{12}–C_{13} stretching character to ~1317 cm^{-1}. The 1248-cm^{-1} C_{12}–C_{13} stretching mode is calculated to shift 77 cm^{-1} to 1331 cm^{-1} upon 14-deuteriation, and the contribution of both the C_{12}–C_{13} and C_{14}–C_{15} stretches to the 1255-cm^{-1} mode drops dramatically. In addition, the C_{14}–C_{15} stretch shifts down 8 cm^{-1} (6 cm^{-1} calculated) from 1201 to 1193 cm^{-1}. Thus, the shifts observed in the 14-D derivative support the assignments of the C_{12}–C_{13} and C_{14}–C_{15} stretches based on the observed ^{13}C shifts. To reproduce the 69-cm^{-1} frequency shift of the C_{12}–C_{13} stretch upon 14-deuteriation, it was necessary to increase the (C–C,C–CH_3) interaction constant. When the *all-trans*-PSB force constant (-0.14 mdyn/Å) is used, the $C_{14}H$ rocking mode was calculated above 1400 cm^{-1} and deuteriation shifted the C_{12}–C_{13} stretch to 1396 cm^{-1}, much higher than observed. Raising this constant to 0.103 mdyn/Å lowered the $C_{14}H$ frequency to 1382 cm^{-1} and reduced the deuterium-induced shift of the C_{12}–C_{13} stretching mode to 77 cm^{-1}.[31]

(29) Curry, B.; Palings, I.; Broek, A. D.; Pardoen, J. A.; Lugtenburg, J.; Mathies, R. *Adv. Infrared Raman Spectrosc.* **1985**, *12*, 115.

(30) Massig, G.; Stockburger, M.; Gaertner, W.; Oesterhelt, D.; Towner, P. *J. Raman Spectrosc.* **1982**, *12*, 287.

(31) The potential interaction between the $C_{14}H$ rock and the C_{12}–C_{13} stretch is dominated by a large positive contribution from the Urey–Bradley term that is ~0.3 mdyn/Å. The non-Urey–Bradley term is used to fine-tune the overall interaction and can reasonably be positive or negative.[23]

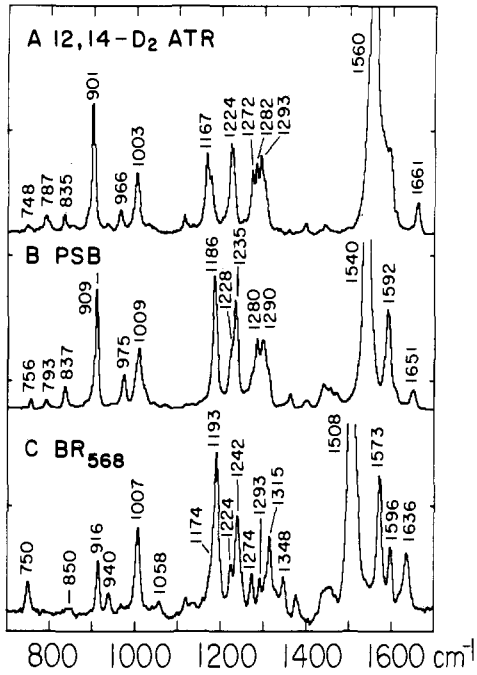

Figure 7. Raman spectra of the 12,14-D_2 derivatives of *all-trans*-retinal (A), the *all-trans* protonated Schiff base (B), and BR_{568} (C).

The 12-D-BR_{568} spectrum is shown in Figure 4F and the calculated normal modes are presented in Table VII. 12-Deuteriation leads to large changes in both the frequencies and intensities of the fingerprint lines. Thus, it is useful to correlate the spectral shifts observed in the pigment with those observed in the [12-D]-PSB (Figure 6B). The 1159-, 1191-, 1204-, and 1237-cm^{-1} lines in the native PSB have been assigned to the C_{10}–C_{11}, C_{14}–C_{15}, C_8–C_9, and C_{12}–C_{13} stretches, respectively.[9] When C_{12} is deuteriated in the PSB, the C_{10}–C_{11} stretch shifts up 7 cm^{-1} to 1166 cm^{-1} and the C_{14}–C_{15} stretch shifts down 2 cm^{-1} to 1189 cm^{-1}. The most dramatic result of 12-deuteriation is a shift of the C_8–C_9 and C_{12}–C_{13} stretches to form an intense symmetric combination at 1242 cm^{-1} and a weak antisymmetric combination at 1218 cm^{-1}. In 12-D-BR_{568}, a similar set of changes are observed. First, we assign the C_{10}–C_{11} stretch at ~1183 cm^{-1} and the C_{14}–C_{15} stretch at 1198 cm^{-1}. This is in agreement with the PSB assignments as well as the BR_{568} calculations which show a moderate upshift of the C_{10}–C_{11} stretch and a slight downshift of the C_{14}–C_{15} stretch (Table VII). The intensities of the 1224- and 1244/1254-cm^{-1} modes in 12-D-BR_{568} closely resemble those observed in the 12-D-PSB. The C_8–C_9 stretch is calculated to shift 16 cm^{-1} to 1234 cm^{-1} where it forms an antisymmetric combination with the C_{14}–C_{15} and C_{12}–C_{13} stretches. The symmetric combination of the C_{12}–C_{13} and C_8–C_9 stretches is calculated at 1250 cm^{-1}. Thus, we assign the 1224- and 1244-cm^{-1} modes to mixed vibrations involving the C_8–C_9 and C_{12}–C_{13} stretches. The 1254-cm^{-1} mode is assigned to the lysine rock which has gained intensity in the 12-D derivative due to mixing with the 1244-cm^{-1} mode.

The spectrum of the 12,14-D_2-BR_{568} derivative is compared with 12,14-D_2-*all-trans*-retinal and its protonated Schiff base in Figure 7. The calculated normal modes for 12,14-D_2-BR_{568} are presented in Table XII. As noted above, deuteriation at C_{14} in BR_{568} results in a 69-cm^{-1} upshift of the C_{12}–C_{13} stretch and a 8-cm^{-1} downshift of the C_{14}–C_{15} stretch. Deuteriation at C_{12} results in a 10-cm^{-1} shift of the C_8–C_9 stretch to 1224 cm^{-1} and a 14-cm^{-1} shift of the C_{10}–C_{11} stretch to 1183 cm^{-1}. Assuming that the effects of these derivatives are additive, we assign the intense line at 1315 cm^{-1} in 12,14-D_2-BR_{568} as the shifted C_{12}–C_{13} stretch, the 1224-cm^{-1} line as the C_8–C_9 stretch, and the 1193-cm^{-1} line as the C_{14}–C_{15} stretch. The 1242-cm^{-1} line is assigned to the lysine rock which has shifted down in frequency and consequently gained intensity by mixing with the higher frequency C_8–C_9 stretch. This mode is calculated to shift down in frequency by 3 cm^{-1} (13 cm^{-1} observed) in the 12,14-D_2 derivative. The C_{10}–C_{11} stretching mode is assigned to the weak shoulder at 1174 cm^{-1}, a shift of 5 cm^{-1} (5 cm^{-1} calculated) from its native frequency. However, on the basis of the 12-monodeuterio shift of 14 cm^{-1}, it is possible that the C_{10}–C_{11} stretch is higher in frequency, degenerate with the intense 1193-cm^{-1} C_{14}–C_{15} stretching mode. In this case, the 1174-cm^{-1} shoulder would correspond to the normal mode observed at this frequency in the 10,11-^{13}C spectrum which is assigned to a vibration of the cyclohexene ring.[16]

Table XII. Calculated Frequencies and Assignments for 12,14-D_2-Substituted BR_{568}

obsd	calcd	description[a]
1636	1638	0.35(C=N) - 0.12(13=14) - 0.56(NH) + 0.47(15H)
	1604	0.33(7=8) - 0.10(5=6)
1596	1597	0.34(5=6) + 0.09(7=8)
1573	1567	0.26(13=14) - 0.20(9=10) - 0.16(5=6)
1514	1525	0.28(9=10) + 0.22(13=14)
1508	1510	0.32(11=12) + 0.14(13=14) - 0.20(12—13)
	1388	0.66(10H) - 0.52(8H) - 0.47(7H)
1348	1353	1.17(NH) + 0.41(15H)
	1342	0.78(15H) - 0.13(14—15)
1327	1327	0.54(7H) + 0.42(8H) - 0.17(12—13)
1315	1317	0.18(12—13) + 0.17(8—9) - 0.18(13-CH_3) - 0.17(9-CH_3)
1293	1307	0.71(7H) - 0.52(8H)
1274	1287	0.90(11H)
1242	1252	0.87(lysine rock) + 0.04(8—9)
1224	1239	0.14(8—9) + 0.13(10—11) - 0.08(14—15)
1193	1196	0.22(14—15) + 0.15(8—9)
1174	1175	0.29(10—11)
	1088	0.21(N—C) + 0.26(12D) - 0.46(14D)
	1031	0.53(12D) - 0.54(20CH_3r) - 0.10(N—C) - 0.09(14D)
	1009	0.49(20CH_3r) - 0.24(N—C) - 0.34(14D) + 0.11(12D)
1007	1002	0.72(19CH_3r) + 0.14(20CH_3r)
916	920	0.54(14D) + 0.51(12D)

[a] See footnotes to Table II.

Deuteriation at C_{11} in BR_{568} (Figure 4G) results in very few frequency changes in the vibrational fingerprint. The C_{10}–C_{11} stretch is calculated to shift 16 cm^{-1} in 11-D-BR_{568} (Table VIII), and intensity changes in the 1170–1210-cm^{-1} region suggest that C_{10}–C_{11} character has shifted to higher frequency. However, in the 11-D-BR_{568} spectrum a vibrational line is still observed at the native C_{10}–C_{11} frequency, suggesting that this stretch is weakly coupled with the $C_{11}H$ rock. In the 11-D-PSB (Figure 6C) a line is observed at the same frequency (1159 cm^{-1}) as the C_{10}–C_{11} stretching mode in the native PSB. These PSB results are consistent with the idea that the $C_{11}H$ rock and C_{10}–C_{11} stretch are not strongly coupled in BR_{568}. However, it should be noted that the residual intensity at the native C_{10}–C_{11} stretch frequency in 11D-BR_{568} may be due to the cyclohexene ring mode discussed above.

The spectral shifts expected in 10-D-BR_{568} (Figure 4I) are analogous to those observed upon 14-deuteriation: a large upshift of the methyl-substituted C_8–C_9 stretch and only a slight shift of the adjacent C_{10}–C_{11} stretch. Thus, in 10-D-BR_{568}, we observe that the C_{10}–C_{11} stretch shifts down in frequency by 5 cm^{-1} to 1165 cm^{-1}, while the C_8–C_9 stretch shifts up 80 cm^{-1} to 1294 cm^{-1}. The C_{12}–C_{13} stretch drops 11 cm^{-1} to 1237 cm^{-1} and gains intensity as a result of interaction with the higher frequency C_8–C_9 stretch, while the C_{14}–C_{15} stretch shifts only slightly to 1204 cm^{-1}. The 1173-cm^{-1} cyclohexene ring line is resolved when the C_{10}–C_{11} stretch drops in frequency. These shifts are reproduced quite well in the calculation (Table IX). The C_{12}–C_{13} and C_{10}–C_{11} stretches are calculated to drop 4 and 3 cm^{-1}, respectively, while the C_8–C_9 stretch is calculated to shift up ~74 cm^{-1}. The isotopic shifts in 10-D-BR_{568} are analogous to those in the 10-D-PSB (Figure 6E). The 1279-cm^{-1} line in the PSB derivative is assigned as the upshifted C_8–C_9 stretch, a shift of 75 cm^{-1}. Similarly, the 1156-cm^{-1} line is assigned as the C_{10}–C_{11} stretching mode, and the 1189 cm^{-1} line as the C_{14}–C_{15} vibration. The C_{12}–C_{13} stretch has shifted 7 cm^{-1} to 1230 cm^{-1} and gained intensity, analogous to the 11-cm^{-1} shift and intensity increase of this mode in the 10-D-BR_{568} derivative.

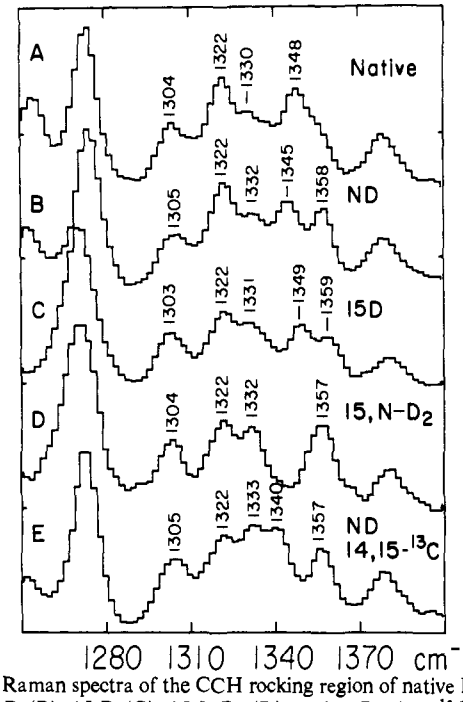

Figure 8. Raman spectra of the CCH rocking region of native BR_{568} (A) and its *N*-D (B), 15-D (C), 15,*N*-D_2 (D), and *N*-D;14,15-$^{13}C_2$ (E) derivatives.

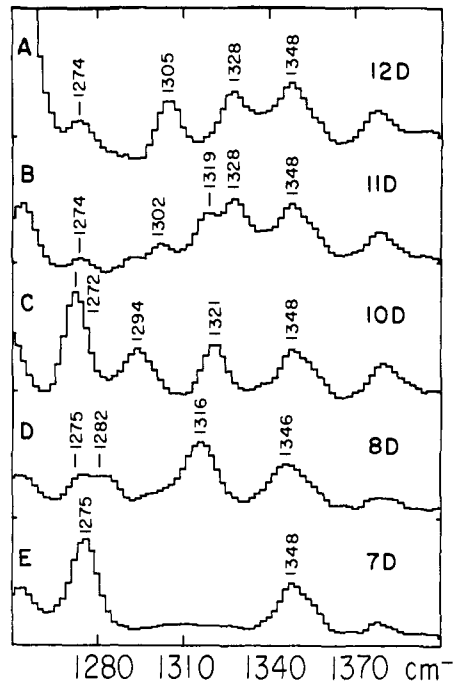

Figure 9. Raman spectra of the CCH rocking region of the 12-D (A), 11-D (B), 10-D (C), 8-D (D), and 7-D (E) derivatives of BR_{568}.

In the spectrum of 8-D-BR_{568} (Figure 4J), the C_8–C_9 stretch shifts up 9 cm^{-1} (9 cm^{-1} calculated) to 1223 cm^{-1} with only slight frequency changes in the other fingerprint vibrations. Intensity changes in the 1169- and 1201-cm^{-1} modes result from reduction of C_8–C_9 stretch character in these modes as the C_8–C_9 stretch shifts to higher frequency. The 1201-cm^{-1} C_{14}–C_{15} stretching mode is calculated to mix in-phase with the C_8–C_9 stretch and loses intensity when the C_8–C_9 stretch character is reduced, while the 1170-cm^{-1} C_{10}–C_{11} stretch mixes out-of-phase with the C_8–C_9 stretch and gains intensity when C_8–C_9 stretch character is reduced (Table X).

No significant changes are observed in the fingerprint region of the 7-D-BR_{568} spectrum (Figure 4K), indicating that the C_7H rock is not coupled with any of the observed C–C stretches. Interestingly, the 1122-cm^{-1} mode which is sensitive to 7-^{13}C substitution shifts only slightly to 1123 cm^{-1} in the 7-D derivative.

Vinyl CCH Rocks. Both ^{2}H- and ^{13}C-substitution can be used to assign the CCH in-plane rocking modes. The most dramatic effect is substitution of the vinyl protons with deuterium. The deuteriated rocks shift out of the fingerprint region of the spectrum to 900–1000 cm^{-1}. However, large changes in frequency and intensity of the *remaining* CCH rocking modes often occur in the deuterium derivatives as a result of the upshift of C–C stretching character and altered mixing among the CCH modes. For this reason it is useful to make use of the sensitivity to ^{13}C-substitution of the CCH modes. The frequency shift of a pure rocking internal coordinate upon ^{13}C-substitution of the central carbon atom is calculated to be ~2 cm^{-1}, but larger shifts are observed due to contributions from kinetically coupled C—C and C=C stretching coordinates.

The 1348-cm^{-1} band is made up of two in-plane rocking modes, the N–H rock at 1348 and the C_{15}H rock at 1345 cm^{-1}. The NH in-plane rock has previously been assigned at ~1348 cm^{-1} by Massig et al.[30] based on a shift of this line to 977 cm^{-1} upon N-deuteriation. We observe a similar shift of the NH rock in our spectra (Figure 8B) leaving the residual C_{15}H rock at 1345 cm^{-1}. The disappearance of the NH rock at 1348 cm^{-1} can be more clearly seen by comparing the 15-D and 15,*N*-D_2 derivatives in Figure 8, C and D. Additional support for this assignment comes from the 4-cm^{-1} shift (5 cm^{-1} calculated) of the 1348-cm^{-1} line in 15-^{13}C-BR_{568} (Figure 2C), presumably as a result of C=N character in the NH rocking mode, and a shift of 3 cm^{-1} in ^{15}N-BR_{568} (Figure 2B). We calculate the NH rock at 1352 cm^{-1} and the ND rock at 974 cm^{-1} very close to the observed frequencies.

Comparison of the *N*-D and 15,*N*-D_2 spectra (Figure 8, B and D) clearly shows a line disappearing at ~1345 cm^{-1} which we assign as the C_{15}H rock. Our calculation places the C_{15}H rock at 1337 cm^{-1} with an out-of-phase contribution from the NH rock. Support for this assignment comes from the 5-cm^{-1} shift (3 cm^{-1} calculated) of the 1345-cm^{-1} line in the 14,15-^{13}C;*N*-D spectrum (Figure 8E) and the 2-cm^{-1} shift to 1343 cm^{-1} in ^{15}N;*N*-D-BR_{568} (data not shown).[16] These shifts are attributed to the C=N and C_{14}–C_{15} stretch character in the normal mode. Assignment of the C_{15}H rock at 1255 cm^{-1}, as initially suggested by Massig et al.,[30] would require an unusually large reduction in the C_{15}H force constant relative to the other CCH rocks in BR_{568}.

Since the C_{14}H rock is strongly coupled with the C_{12}–C_{13} stretch, its assignment is complicated by the upshift of the C_{12}–C_{13} stretching mode to 1317 cm^{-1} when C_{14} is deuteriated. In *all-trans*-retinal, the C_{14}H rocking mode was assigned at 1334 cm^{-1} on the basis of its 13-cm^{-1} shift to 1321 cm^{-1} in the 13-^{13}C derivative. This shift reflects the large C_{12}–C_{13} stretching component in this normal mode.[29] In 13-^{13}C-BR_{568} (Figure 2F), no shifts of similar magnitude are observed in the CCH rocking region. A shift of the 1322-cm^{-1} line to 1318 cm^{-1} is observed but is attributed to C_{12}–C_{13} character in the C_{12}H rocking mode (see below). The C_{14}H rock is calculated at 1382 cm^{-1}, but no intensity changes are observed near this frequency in the 14-D spectrum. The high frequency calculated for the C_{14}H rock relative to its frequency in ATR is a result of the force field changes which were required to raise the frequency of the C_{12}–C_{13} stretch. The C_{14}D frequency cannot be clearly assigned but most likely contributes to the 972- and/or 984-cm^{-1} modes in the 14-D spectrum. The appearance of two low-frequency lines in the 14-D spectrum probably results from mixing of the 7,8 A_u HOOP mode with the nearly degenerate C_{14}D rock. The deuteriated rock is calculated at 973 cm^{-1}, suggesting that the frequency of the protonated rock may be approximately correct. Only in the 12,14-D_2 derivative is the C_{14}D rock clearly assigned, where it forms a symmetric combination with the C_{12}D rock at 916 cm^{-1} (920 cm^{-1} calculated). The increased frequency of the C_{14}D + C_{12}D combination relative to *all-trans*-retinal (901 cm^{-1}, Figure 7A) suggests that the protonated 12 and 14 rocks are higher in BR_{568} than in retinal.

The C_{12}H rock is assigned at 1322 cm^{-1} on the basis of intensity loss at this position in the 12-D-BR_{568} derivative (Figure 9A). This assignment is supported by the 4–5-cm^{-1} shift of this line

in the 11-, 12-, and 13-^{13}C derivatives. The frequency of the $C_{12}H$ rock is much higher than in *all-trans*-retinal (1302 cm^{-1}). This frequency increase may result from an increase in the ($C_{12}H$,-C_{12}–C_{13}) coupling because the C_{12}–C_{13} stretching vibration is 32 cm^{-1} higher in BR than in ATR. This would predict a larger ^{13}C shift in the $C_{12}H$ rock in BR_{568} than in ATR. This is in fact observed; a 4-cm^{-1} shift is observed in the $C_{12}H$ rock in 13-^{13}C-BR, whereas the $C_{12}H$ rock shifts only 1 cm^{-1} in the 13-^{13}C-ATR. The $C_{12}H$ rocking mode is calculated at 1314 cm^{-1} as a symmetric combination of the $C_{11}H$ and $C_{12}H$ rocks. However, the predicted coupling between the $C_{11}H$ and $C_{12}H$ rocks is much larger than is observed. To reduce this coupling, and thus the large shifts of the $C_{11}H$ rock in the 12-D calculation and of the $C_{12}H$ rock in the 11-D calculation, it would be necessary to selectively iterate the rock–rock coupling constants. Finally, the $C_{12}D$ rocking mode is assigned at 980 cm^{-1} (979 cm^{-1} calculated).

In the 12,14-D_2 derivative of BR_{568}, direct kinetic coupling splits the individual $C_{12}D$ and $C_{14}D$ rocking modes into a symmetric combination which is calculated at 920 cm^{-1}, and an antisymmetric combination which is calculated to mix with the $C_{20}H_3$ methyl rock and N–C stretch to form normal modes at 1009, 1031, and 1088 cm^{-1}. Only the symmetric combination is observed in the 12,14-D_2-BR_{568} Raman spectrum where it appears as an intense band at 916 cm^{-1} (Figure 7C).

The $C_{11}H$ rock is assigned at 1273 cm^{-1} on the basis of a shift of this mode to 960 cm^{-1} upon 11-deuteriation. Both the protonated and the deuteriated rocking vibrations are similar to those in *all-trans*-retinal (1270 and 966 cm^{-1}) and the *all-trans*-PSB (1273 and 968 cm^{-1}). A weak mode remains at 1274 cm^{-1} in the 11-D-BR_{568} derivative which has not been assigned (Figure 9B).

The $C_{10}H$ in-plane rock, calculated at 1395 cm^{-1}, has not been observed in the native BR_{568} spectrum. The shift of C_8–C_9 stretching character into the region of the CCH rocks in the 10-D derivative results in loss of intensity in normal modes at 1305 and 1330 cm^{-1} (Figure 9C). However, on the basis of the isotopic shifts observed in the 7-D and 8-D-BR_{568} derivatives, we have assigned these lines to the C_7H and C_8H rocks which form a symmetric combination at 1330 cm^{-1} and an antisymmetric combination at 1305 cm^{-1} (below). One explanation for the sensitivity of these modes to 10-deuteriation is provided by the calculation (Table IX). When the C_8–C_9 stretch shifts up in frequency upon 10-deuteriation, the symmetric combination of the C_7H and C_8H rocks is calculated to shift to 1359 cm^{-1} while the antisymmetric combination mixes with the C_8–C_9 stretch forming an intense mode at 1294 cm^{-1}, where the rock–stretch intensities add, and a weak mode calculated at 1306 cm^{-1}, where the rock–stretch intensities cancel. The 9-^{13}C spectrum shows no significant frequency shifts of the CCH rocking modes which may be used to assign the $C_{10}H$ rock. Examination of the observed lines near the calculated 1395-cm^{-1} frequency shows no effects resulting from 10-deuteriation. The only quantitative information is the observation of the $C_{10}D$ in-plane rock at 972 cm^{-1} (970 cm^{-1} calculated).

The C_7H and C_8H in-plane rocks are calculated to be strongly mixed, forming a symmetric combination at 1325 cm^{-1} and an antisymmetric combination at 1303 cm^{-1}. In the 7-D-BR_{568} spectrum (Figure 9E), intensity is lost at 1305, 1322, and 1330 cm^{-1}, while in the 8-D derivative (Figure 9D), intensity is lost at 1305 cm^{-1} and intensity has shifted from 1322–1330 cm^{-1} to 1316 cm^{-1}. We assign the symmetric combination of the C_7H and C_8H rocks to the 1330-cm^{-1} line and the antisymmetric combination to the line at 1305 cm^{-1}. The C_7H rocking coordinate is calculated to make significant contributions to both modes in agreement with the loss of intensity between 1275 and 1348 cm^{-1} in the 7-D-BR_{568} spectrum. In contrast, upon 8-deuteriation, the uncoupled C_7H rock forms an intense mode at 1316 cm^{-1} (1317 cm^{-1} calculated), while the C_8D rock has shifted to 980 cm^{-1}. ^{13}C-Substitution lends support to these assignments. In the 7- and 8-^{13}C derivatives, the 1330 cm^{-1} line shifts ~10 cm^{-1} to 1320 cm^{-1} reflecting contributions from the C_6—C_7, C_7=C_8, and/or C_8—C_9 stretches.

(B) Hydrogen Out-of-Plane Vibrations. Table XIII presents the vinyl hydrogen out-of-plane wag assignments for BR_{568}. The HOOP assignments are aided by vibrational calculations and by comparisons with model compounds. On the basis of empirical assignments and normal mode calculations for these vibrations in *all-trans*-retinal, Curry et al. formulated four general rules for HOOP frequencies in trans-substituted polyenes.[8] (1) Hydrogens trans to a double bond couple strongly forming an "A_u" HOOP in the 950–970-cm^{-1} range and a "B_g" HOOP from 750 to 850 cm^{-1}. (2) A proton and a deuteron trans across a double bond give rise to two lines, one due to the largely uncoupled protonated wag (900–920 cm^{-1}) and the other due to the deuteriated wag (700–750 cm^{-1}). (3) Deuterons trans to a double bond couple weakly or not at all with each other. (4) A proton trans to a CH_3 group across a double bond appears between 850 and 900 cm^{-1}.

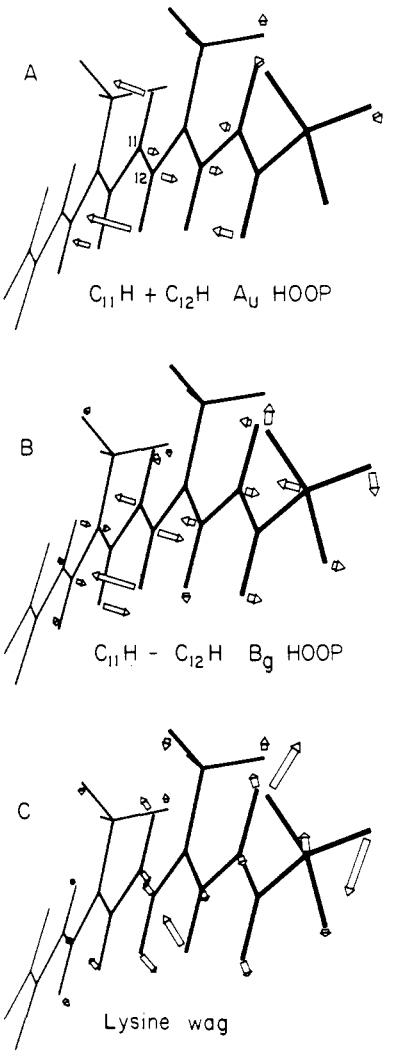

Figure 10. Mass-weighted atomic displacements of the calculated 968 (A), 832 (B), and 818 cm^{-1} (C) HOOP modes of BR_{568}.

The trans HC_{11}=$C_{12}H$ protons in BR_{568} couple strongly to form an A_u HOOP at 959 cm^{-1} and a B_g HOOP at ~840 cm^{-1}. The atomic displacements of these modes are depicted in Figure 10. The A_u HOOP assignment at 959 cm^{-1} (968 cm^{-1} calculated) is based on the disappearance of this line in 12-D and 12,14-D_2-BR_{568} (Figures 4F and 7C). In the 11-D spectrum (Figure 4G), the $C_{11}D$ in-plane rock has shifted to 960 cm^{-1}, making it appear as though the 959-cm^{-1} line is not sensitive to 11-deuteriation. There are two weak lines at ~842 and 851 cm^{-1} (see Figure 11A) which could be the B_g HOOP mode. We tentatively assign the 842-cm^{-1} mode to the HC_{11}=$C_{12}H$ B_g vibration based on its correspondence with the calculated frequency.

In 11-D-BR_{568}, the uncoupled $C_{12}H$ wag is calculated to shift to 930 cm^{-1} (926 cm^{-1} observed), while the $C_{11}D$ wag is calculated at 743 cm^{-1}. A weak line is observed at 744 cm^{-1} in the 11-D spectrum close to the calculated frequency. However, a weak line is also observed at this position in the native spectrum (Figure 11) precluding a conclusive assignment. In 12-D-BR_{568}, the

Table XIII. Calculated Frequencies and Assignments for Hydrogen Out-of-Plane Wags[a]

obsd	calcd	description	obsd	calcd	description
		Unmodified			12,14-D_2
1002	1009	0.98(15w) - 0.16(lysine)		1008	0,97(15w)
985	987	0.70(7w) + 0.63(8w)		948	1.07(Nw)
959	968	0.71(12w) + 0.53(11w)		821	0.71(lysine)
942	949	1.04(Nw) + 0.32(lysine)	750	749	0.82(12w) + 0.48(14w)
898	901	0.87(10w)	673	680	0.79(14w) - 0.46(12w)
882	881	0.71(14w) + 0.58(12w) - 0.55(11w)			
851	859	0.71(8w) - 0.60(7w)			12D
842	832	0.68(12w) - 0.49(11w) - 0.63(14w)	940	949	1.05(Nw)
830	818	0.64(lysine) - 0.24(11w) - 0.23(12w) - 0.13(Nw) + 0.28(15w)	918	918	0.72(11w) + 0.61(10w)
				900	0.76(10w) - 0.79(11w)
		15D	856	866	0.85(14w)
	987	0.70(7w) + 0.63(8w)	846	859	0.54(7w) - 0.64(8w)
960	969	0.54(11w) + 0.71(12w)	830	819	0.70(lysine)
943	950	1.03(Nw) + 0.33(lysine)		722	0.92(12w)
896	901	0.87(10w) - 0.58(11w) + 0.47(8w)			
882	884	0.77(14w) + 0.51(12w) - 0.48(11w)			11,12-D_2
	865	0.55(8w) - 0.47(7w) + 0.31(lysine)		987	0.67(7w) + 0.65(8w)
853	856	0.40(lysine) - 0.50(8w)		950	1.05(Nw)
846	832	0.48(11w) - 0.66(12w) - 0.26(lysine)	905	907	0.97(10w)
786	782	0.74(15w)	858	867	0.92(14w)
			845	860	0.61(7w) - 0.71(8w)
		ND	830	819	0.70(lysine)
996[b]	1004	1.02(15w)	742	746	0.86(11w) - 0.55(12w)
	987	0.70(7w) + 0.63(8w)	710	712	0.74(12w) + 0.32(11w)
959	968	0.53(11w) + 0.71(12w)			
896	901	0.86(10w)			11D
887	885	0.80(14w)		950	1.04(Nw)
853	862	0.71(8w) - 0.60(7w)	926	930	0.84(12w) + 0.69(10w)
	849	0.66(lysine)	889	891	0.58(10w) - 0.54(12w)
845	832	0.48(11w) - 0.67(12w)		860	0.71(14w) + 0.62(8w) - 0.53(7w)
722	725	0.78(Nw)	840	848	0.32(7w) - 0.37(8w) + 0.70(14w)
				819	0.70(lysine)
		15,N-D_2	744	743	0.91(11w)
	987	0.70(7w) + 0.63(8w)			
960	968	0.54(11w) + 0.71(12w)			10D
	906	0.46(lysine)		987	0.71(7w) + 0.63(8w)
896	901	0.88(10w)	953	961	0.60(11w) + 0.72(12w)
885	876	0.43(14w)		949	1.02(Nw)
853	858	0.57(7w) - 0.66(8w)	885	884	0.70(14w) - 0.71(11w) + 0.62(12w)
844	832	0.48(11w) - 0.67(12w)		876	0.82(7w) - 0.95(8w)
798	783	0.72(15w)	839	841	0.56(11w) - 0.57(12w) + 0.80(14w)
725	715	0.79(Nw)	830	818	0.68(lysine)
			725[b]	716	0.89(10w)
		14D			
	1009	0.99(15w)			8D
	987	0.70(7w) + 0.63(8w)	961	968	0.53(11w) + 0.70(12w)
958	968	0.55(11w) + 0.70(12w)	939	940	1.06(7w)
	948	1.07(Nw)	898	895	0.92(10w) - 0.74(11w)
898	901	0.88(10w)	881	876	0.79(14w)
850	869	0.69(8w) - 0.57(7w)	743	744	0.94(8w)
840	847	0.68(12w) - 0.56(10w) - 0.41(11w)			
829	820	0.71(lysine)			7D
691	696	0.90(14w)	963	968	0.52(11w) + 0.70(12w)
			930	926	1.02(8w)
			890	889	0.71(10w) - 0.75(11w) + 0.43(14w)
			875	873	0.73(14w) - 0.67(10w)
			675?	761	0.95(7w)

[a] Abbreviations used: w, hydrogen out-of-plane wag. [b] Frequency obtained from 77 K spectrum.

uncoupled $C_{11}H$ wag is found at 918 cm^{-1} (918 cm^{-1} calculated). The 12-D wag is most clearly observed at 750 cm^{-1} in 12,14-D_2-BR_{568} (Figure 7C) where it mixes with the $C_{14}D$ wag and is presumably pushed up in frequency from its position in 12-D-BR_{568}. In 11,12-D_2-BR_{568}, the $C_{12}D$ and $C_{11}D$ wags are calculated to form an antisymmetric combination at 746 cm^{-1} (742 cm^{-1} observed) and a symmetric combination at 712 cm^{-1} (710 cm^{-1} observed). However, the assignment of the 742-cm^{-1} mode is not definitive due to the presence of weak lines in the native spectrum (Figure 11).

We calculate the $HC_7{=}C_8H$ A_u HOOP combination at 987 cm^{-1} and a $\mathbf{B_g}$ combination at 859 cm^{-1}. There are two weak lines near 987 cm^{-1} (i.e., 971 and 984 cm^{-1} in Figure 11A) which are candidates for this A_u HOOP mode. However, neither line shifts in 7- or 8-^{13}C-BR_{568}, and these lines cannot be resolved in the 7-D or 8-D spectra due to the appearance of the C_7D and C_8D in-plane rocks. The uncoupled C_7H and C_8H HOOP modes in the 8-D and 7-D derivatives are assigned to weak lines at 939 and 930 cm^{-1}, respectively. These frequencies are close to the values expected for uncoupled protonated wags based on the rules given above, and they are reproduced in the calculation. The C_8D wag is assigned at 743 cm^{-1} (744 cm^{-1} calculated) in the 8-D-BR_{568} spectrum. The C_7D wag assignment is more ambiguous. Three very weak modes are observed at 675, 713, and ~748 cm^{-1}, with the 675-cm^{-1} line becoming quite intense in the 7,8-D_2 spectrum. The shift of the 675-cm^{-1} line to 672 cm^{-1} in the 7,8-D_2 spectrum and its increased intensity suggest that the 675-cm^{-1} mode is the C_7D wag. This assignment places this mode significantly below the C_7D frequency in ATR (718 cm^{-1}). The calculation which was not fit to the 675-cm^{-1} assignment predicts a C_7D frequency of 761 cm^{-1}.

The $C_{10}H$ wag is assigned at 898 cm^{-1} on the basis of a shift to 725 cm^{-1} (716 cm^{-1} calculated) in 10-D-BR_{568}. The $C_{10}D$ wag is not observed in the 10-D-BR_{568} spectrum (Figure 4I), but it

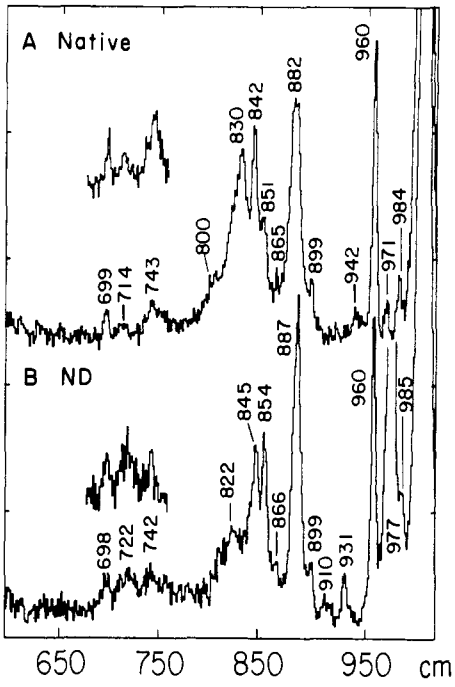

Figure 11. High signal-to-noise spectra of the low wavenumber region of native BR_{568} in H_2O (A) and D_2O (B). Inserts are replicate scans.

appears as a weak line at 725 cm^{-1} in the 77 K 10-D spectrum.[15] The $C_{14}H$ wag is assigned at 882 cm^{-1} on the basis of a shift to 691 cm^{-1} (696 cm^{-1} calculated) in 14-D-BR_{568} (Figure 4E). The $C_{10}H$ and $C_{14}H$ frequencies and isotopic shifts are close to those observed in *all-trans*-retinal.

The Schiff base moiety is thought to have a central role in the proton pumping mechanism of bacteriorhodopsin, so it is important to examine the NH and $C_{15}H$ wags in detail. The simplest picture is one in which the $C_{15}H$ and NH protons couple across the C=N bond to form a high-frequency "A_u" and a low-frequency "B_g" combination. However, hydrogen bonding of the Schiff base proton may alter its vibrational properties. Also, the vibrational coupling between the NH wag and out-of-plane modes of the ϵ-lysine CH_2 group may alter the frequency and isotopic shifts of the NH and $C_{15}H$ HOOP modes. Thus, it is difficult to predict a priori the frequencies and coupling patterns of these vibrations.

We will first deal with the assignment of the ND and $C_{15}D$ wags. Deuteration at C_{15} produces an intense band at 786 cm^{-1} which can immediately be assigned as the $C_{15}D$ wag (Figure 4C). The appearance of an intense $C_{15}D$ *in-plane* rock at 974 cm^{-1} makes the assignment of the $C_{15}H$ wag difficult. Loss of intensity at 985 and 1002 cm^{-1} in high signal-to-noise 15-D spectra of Massig et al.[30] suggests that the $C_{15}H$ wag is higher in frequency than the protonated wags previously discussed. N-Deuteriation (Figure 11) results in loss of intensity in the strong 830-cm^{-1} line and in a much weaker line at 942 cm^{-1}. There is an intensity increase at 722 cm^{-1} in the ND spectrum which is tentatively assigned as the ND wag. This assignment is consistent with shifts in other derivatives. The ND wag must be *below* 786 cm^{-1} because in 15,*N*-D_2 BR_{568} (Figure 4D) the $C_{15}D$ wag is pushed *up* to 798 cm^{-1} due to coupling with the lower frequency ND HOOP mode. Similarly, the ND wag must be *above* ~690 cm^{-1} because the $C_{14}D$ wag at 691 cm^{-1} in the 14D spectrum shifts down to 678 cm^{-1} in the 14,*N*-D_2 spectrum due to coupling with the ND wag. A drop in the $C_{14}D$ wag frequency is also observed in the 12,14,*N*-D_3 spectrum (data not shown) along with the appearance of a weak broad line at ~707 cm^{-1} which could correspond with the ND wag.[16] These shifts argue that the ND wag is at ~720 cm^{-1}.

Several lines of evidence forced us to abandon the earlier assignment of the 830-cm^{-1} line as an isolated N—H wag or HN=$C_{15}H$ wag combination.[32] First, if the same H/D frequency ratio observed for C–H wags (~1.24–1.28) is applied to the N–D wag, the 722 cm^{-1} N–D frequency predicts an N–H frequency significantly above 830 cm^{-1}. Second, the assignment of the NH wag at 830 cm^{-1} is inconsistent with the isotopic induced shift of the $C_{14}H$ wag upon N-deuteriation. If the NH wag (or HN=$C_{15}H$ B_g combination) is *below* the $C_{14}H$ wag then the $C_{14}H$ wag will *drop* in frequency upon N-deuteriation. If the NH wag is *above* the $C_{14}H$ wag, the $C_{14}H$ wag will *increase* in frequency in *N*-D-BR_{568}. Thus, the 5-cm^{-1} upshift of the $C_{14}H$ mode to 887 cm^{-1} observed in D_2O argues that the NH wag is above 882 cm^{-1}.

If the 830-cm^{-1} mode is not the NH wag, then we must account for intensity changes at this frequency in *N*-D-BR_{568} and assign the NH wag to another position. One explanation for the sensitivity of the 830-cm^{-1} mode to N-deuteriation is that it is predominantly the out-of-plane vibration of the lysine CH_2 group, which contains some NH character due to vibrational coupling. This mode is depicted in Figure 10C. We are able to calculate this mode near 830 cm^{-1} using reasonable force constants for the lysine coordinates. Upon N-deuteriation, this mode is calculated to shift 31 cm^{-1} to 849 cm^{-1}. Comparing the NH and ND spectra in Figure 11 reveals a large increase of intensity at 854 cm^{-1} which may be attributed to the 830-cm^{-1} mode shifting to higher frequency when coupling with the NH wag is removed.[33]

If we assign the 830-cm^{-1} mode to the lysine vibration and then iterate the out-of-plane force field to reproduce the frequencies and shifts of the $C_{15}D$ and $C_{14}D$ wags in the various derivatives discussed above, the $C_{15}H$ and NH wags are calculated at 1009 and 949 cm^{-1}, respectively.[34] The 1009-cm^{-1} line is close to the 1002-cm^{-1} shoulder which disappears upon 15-deuteriation[30] and is therefore assigned as the $C_{15}H$ wag. Raman spectra of *N*-D-BR_{568} at 77 K suggest that this line shifts to 996 cm^{-1} consistent with an assignment as a weakly coupled HC_{15}=NH "A_u" combination. This shift is reproduced in the calculation. The calculated 949-cm^{-1} frequency is close to that of the 942-cm^{-1} line which loses intensity upon N-deuteriation (Figure 11B). This line appears to increase in intensity in the 15-D spectrum (Figure 4C) which would be consistent with its assignment as a weakly coupled HC_{15}=NH combination.

(C) Methyl-Group Vibrations. The methyl-group vibrations of BR_{568} are very similar to those of *all-trans*-retinal and the *all-trans*-PSB. These vibrations can be divided into three categories: the HCH bending vibrations or methyl deformations, the methyl rocks, and the C–CH_3 stretches. The broad band at ~1450 cm^{-1} in native BR_{568} is due to the asymmetric deformations of the methyl groups, while the 1378-cm^{-1} line results from the symmetric deformations. These assignments are based on their

(32) Attempts to fit the NH wag (or NH=$C_{15}H$ "B_g" combination) at 830 cm^{-1} in the vibrational calculation were frustrated by interaction of the lysine mode and the NH mode. For instance, if the diagonal NH force constant was lowered, both the lysine mode and the NH mode would drop in frequency and begin to exchange character. When the NH force constant was decreased enough to produce the 830-cm^{-1} frequency, exchange of character between these modes was significant with the majority of the NH character appearing at ~750 cm^{-1}. To test whether incorrect geometric or potential energy parametrization of the lysine group prevented the calculation of the 830-cm^{-1} line as the NH wag, out-of-plane calculations were undertaken on an *all-trans*-retinal PSB terminating in a C=NH—R group. The out-of-plane force field was adjusted to place the NH wag at ~830 cm^{-1}. The observed couplings between the NH, $C_{15}H$, and $C_{14}H$ wags were approximately reproduced. However, the calculation still incorrectly predicted the *direction* of the shift of the $C_{14}H$ wag upon N-deuteriation (882 → 880 cm^{-1} calculated, 882 → 887 cm^{-1} observed). Further, it was not possible to simultaneously fit the $C_{15}H$ wag at ~1002 cm^{-1} and reproduce both the $C_{14}H$ and NH frequencies and isotopic shifts.

(33) The frequency shift of the lysine CH_2 mode upon N-deuteriation is sensitive to the conformation about the N–C_{lys} bond. In the syn geometry, much greater coupling between the NH wag and lysine mode occurs and the lysine mode shifts up ~75 cm^{-1} upon N-deuteriation. The smaller shift (830 → 854 cm^{-1}) observed in BR_{568} suggests that the N–C_{lys} conformation is anti, as depicted in Figure 1.

(34) The frequency ordering and coupling of the lysine–CH_2 mode and the NH wag predicted in the calculations presented here are supported by QCFF-π calculations which predict mixed lysine–CH_2 and NH wag normal modes at 797 and 851 cm^{-1} with the lower frequency mode dominated by the lysine out-of-plane coordinate.

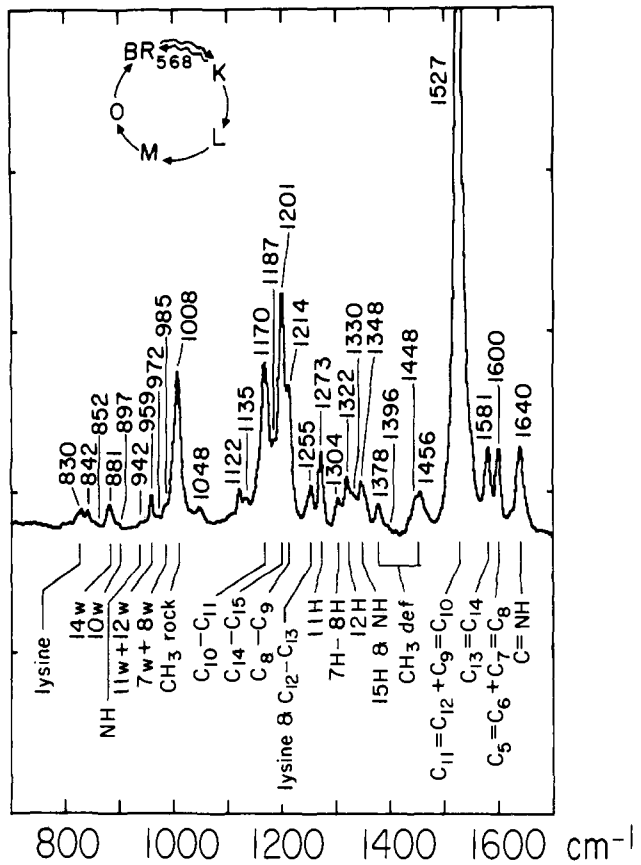

Figure 12. Resonance Raman spectrum of BR_{568} labeled with the dominant internal coordinates that contribute to the vibrational lines.

correspondence with the 1455- and 1389-cm^{-1} methyl deformations in ATR[8] and with the calculated frequencies of ~1450 and 1378 cm^{-1}, respectively.

The 1008-cm^{-1} line has been assigned as the symmetric in-plane rocking combination involving mainly the C_{19} and C_{20} methyl groups. The methyl rocking coordinates couple only weakly, and the asymmetric combination forms a weak mode at 1022 cm^{-1}. When either the C_{19} or C_{20} methyl groups is perdeuterated, the substituted in-plane rock shifts to ~850 cm^{-1}, leaving the remaining in-plane methyl rock at 1016 cm^{-1} in the 10,19-D_4 derivative and at 1019 cm^{-1} in 14,20-D_4 BR_{568}.[15,16]

Finally, the methyl stretches are calculated at 877 and 860 cm^{-1}. However, there are no significant shifts in the major lines in the low-wavenumber region of 18-, 19-, and 20-^{13}C-BR_{568} (data not shown),[16] and thus the C–CH_3 stretching modes have not been assigned.

(D) **Cyclohexene Ring Vibrations.** The vibrations of the cyclohexene ring are generally weak or absent in Raman spectra of BR_{568} because they are only slightly coupled to the resonant $\pi \rightarrow \pi^*$ electronic transition. In the spectrum of the *all-trans*-PSB, three Raman lines at 792, 1121, and 1131 cm^{-1} were attributed to ring modes. These lines correspond well with the weak ~800-, 1122-, and 1135-cm^{-1} lines in BR_{568}. Assignment of the 1122- and 1135-cm^{-1} lines as cyclohexene ring modes is supported by their sensitivity to 5- and 6-^{13}C substitution. Three additional lines at 1174, 1187, and 1203 cm^{-1} (beneath the intense 1201-cm^{-1} C_{14}–C_{15} stretching mode) may result from ring vibrations corresponding to the 1172-, 1187-, and 1206-cm^{-1} modes observed in β-ionone. Of these, the 1187-cm^{-1} line shifts 5 cm^{-1} to 1182 cm^{-1} in the 5-^{13}C derivative and must therefore possess significant C_4–C_5 stretching character.

Discussion

First, it is important to note that the complete vibrational analysis presented here (summary in Figure 12) fully supports

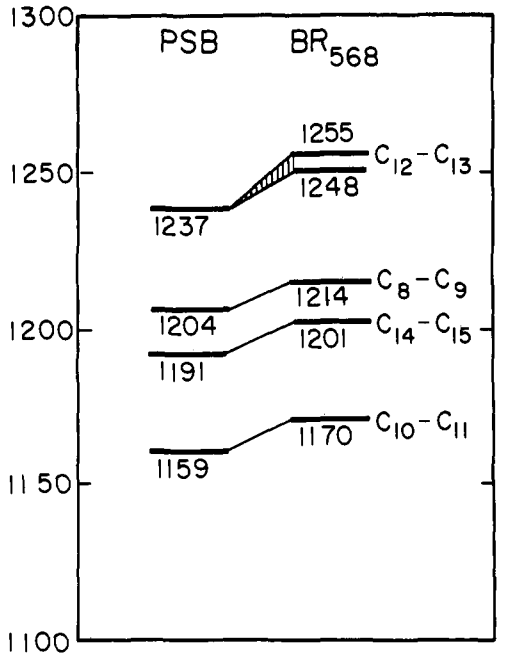

Figure 13. Correlation diagram of the C–C single bond stretches of BR_{568} and the *all-trans* protonated Schiff base (PSB). In BR_{568} the "C_{12}–C_{13} stretch" shifts up and mixes strongly with a lysine–CH_2 rock, producing two modes at 1248 and 1255 cm^{-1}.

the C_{15}=N anti structure of the retinal chromophore in BR_{568}. We previously used calculations on Schiff base fragments to argue that the coupling between the N—H rock and the C_{14}—C_{15} stretch was diagnostic of the C_{15}=N configuration.[22a] N-Deuteriation resulted in a large (>40 cm^{-1}) shift of the C_{14}–C_{15} stretch in the syn geometry and only a small shift in the anti geometry. The calculation presented here which accurately fits the frequencies of the full chromophore and its isotopic derivatives supports this analysis. Also, attempts to reproduce the vibrational frequencies of BR_{568} with use of the syn geometry were unsuccessful. The correctness of this result is further supported by the vibrational analysis of the C_{15}=N syn chromophore in BR_{548}.[35] The BR_{548} calculation, which reproduces the vibrational frequencies of native BR_{548} and its isotopic derivatives, predicts a 45-cm^{-1} upshift of the C_{14}–C_{15} mode upon N-deuteriation—close to the 41-cm^{-1} shift observed.

The vibrational properties of the Schiff base moiety are of interest because the Schiff base proton is thought to be involved in proton pumping. The Schiff base mode is significantly lower in BR_{568} (1640 cm^{-1}) than in the *all-trans*-PSB (1654 cm^{-1}). On the basis of the *N*-D and 15-D shifts in both the *all-trans*-PSB and BR_{568}, we showed in a previous paper[9] that this 14-cm^{-1} frequency difference can be partitioned into 7 cm^{-1} due to reduced N–H rock coupling, 2 cm^{-1} due to reduced C_{15}H rock coupling, and ~5 cm^{-1} due to a reduction in the intrinsic bond order or indirect interactions. The largest effect, a reduction in NH coupling, may be correlated with a reduction in hydrogen bonding between the Schiff base proton and its counterion as shown by solid-state NMR[36] and resonance Raman spectroscopy.[37] The reduced N–H bond length in a weak hydrogen bond is expected to decrease the net rock–stretch coupling; a shorter N–H bond length *increases* the through-space interaction between C_{15} and the Schiff base proton which counteracts the direct kinetic coupling between the NH rock and C=N stretch. This suggests that the magnitude of the shift of the Schiff base mode in D_2O may provide

(35) Smith, S. O.; Pardoen, J. A.; Lugtenburg, J.; Mathies, R. A. *J. Phys. Chem.* **1987**, *91*, 804.

(36) Harbison, G. S.; Herzfeld, J.; Griffin, R. G. *Biochemistry* **1983**, *22*, 1.

(37) Hildebrandt, P.; Stockburger, M. *Biochemistry* **1984**, *23*, 5539.

a probe for changes in Schiff base hydrogen bonding in retinal pigments.[38]

Figure 13 correlates the observed C–C stretching frequencies in BR_{568} with those in the *all-trans*-PSB. The most striking feature of this correlation is that the frequency ordering and spacing is the same in each molecule, and that the frequencies are ~ 10 cm^{-1} higher in BR_{568}. Since *s-trans* → *s-cis* isomerization about the C_{10}–C_{11} or C_{14}–C_{15} bonds would lower the associated C–C stretching frequency by ~ 100 cm^{-1},[39] the increased frequency of these modes in BR_{568} argues that these bonds are in the *s-trans* conformation. The increase of the C–C stretching frequencies is best attributed to increased C–C bond order due to electron delocalization of the conjugated π-system. The delocalized electronic structure is presumably responsible for the shift in the chromophore's absorption maximum from 440 nm in the PSB to 568 nm. This opsin shift has recently been shown to result from at least three factors. First, isomerization of the C_6–C_7 bond from 6-*s-cis* in the PSB to 6-*s-trans* in BR_{568} allows the π-electrons in the C_5=C_6 bond to more fully conjugate with the retinal chain.[10-12,40] The shift of the absorption maximum upon *s-cis* (nonplanar) → *s-trans* (planar) isomerization is expected to be ~ 25 nm.[40,41] Second, a negative bacteriorhodopsin charge (or the minus end of a dipole) placed near C_5 of the retinal chromophore pushes the π-electrons toward the Schiff base and stabilizes positive charge at C_5.[10,42] The influence of this perturbation is diminished by the presence of a *positive* bacteriorhodopsin residue (or the positive end of a dipole) near C_7.[10] Finally, a weakened hydrogen bond between the Schiff base proton and its protein counterion[36,37] enhances delocalization by reducing the stability of positive charge at the Schiff base. It now appears that the latter factor is the dominant contributor to the opsin shift in BR_{568}.[11,12] The observation that *each* C–C stretching frequency shifts ~ 10 cm^{-1} is in agreement with the idea that π-electron delocalization is generated by protein effects at the two "poles" of the retinal chromophore, the Schiff base and the ionone ring. The 11–18-cm^{-1} upshift of the "C_{12}–C_{13} stretch" in the protein provides only weak evidence for this picture since this mode is quite delocalized. This delocalization arises because the C_{12}–C_{13} stretch is the highest frequency C–C mode and consequently couples most strongly with the CC–H rocks. The alternative idea that protein perturbations localized at C_{12} or C_{13} are responsible for the shift of the C_{12}–C_{13} mode is not likely since no large protein perturbations are observed in the ^{13}C NMR chemical shifts of BR_{568} in the C_{12}–C_{13} region.[10]

The Raman intensities of the C=C stretching fundamentals of BR_{568} can also provide useful information about chromophore structure and environment. The observed intensity of a C=C stretching mode is directly related to bond length changes upon electronic excitation. The spectra presented here make it clear that the largest ground → excited state geometry changes in BR_{568} are associated with the central double bonds in the chain. For example, the 1491-cm^{-1} line in 11,12-D_2-BR_{568} is a fairly localized C_{11}=C_{12} stretch and it carries the majority of the Raman intensity. A similar qualitative analysis of other modes in native BR_{568} can be made if they are sufficiently localized to avoid mode mixing effects. The weak intensity of the Schiff base mode suggests that the C_{15}=N bond undergoes small changes upon excitation. Similarly, the C_5=C_6 stretching fundamental at 1600 cm^{-1} has essentially no Raman intensity. These results can now be compared with theoretical calculations on BR_{568}. Kakitani et al.[43] calculated the properties of the BR chromophore with a negative point charge near the ionone ring. They predict ground → excited state changes in bond length of 0.027 and 0.028 Å for the C_5=C_6 and C=N bonds and somewhat smaller changes for the C_9=C_{10} and C_{11}=C_{12} bonds (0.023 and 0.021 Å, respectively). The qualitative discrepancy between the calculated bond length changes and our observed intensities cannot be resolved by mode mixing effects. The insensitivity of the Schiff base mode to ^{13}C labeling of the other C=C stretches shows that the C=N vibration is not highly mixed with other C=C stretching internal coordinates which cancel its intrinsic intensity. Similarly, the $^{13}C_5$ and $^{13}C_6$ data indicate that the C_5=C_6 stretching coordinate is not mixed with other more intense C=C stretches. Thus the C=C mode Raman intensities suggest that the calculations in ref 43 do not provide an accurate description of the electronic structure of the chromophore in BR_{568}.

The intensities of the hydrogen out-of-plane modes provide another probe of chromophore structure in BR_{568}. HOOP modes are expected to be weak in intensity in the Raman spectrum of a planar chromophore. However, these lines can be strongly enhanced by torsional deformations. Strong HOOP vibrations are observed in the Raman spectra of bacteriorhodopsin's K_{625} and O_{640} intermediates,[14,44] and in bathorhodopsin,[45] the primary photoproduct of the visual pigment rhodopsin. The absence of intense HOOP modes in BR_{568} indicates that the chromophore is not strongly torsionally distorted.

Although the HOOP intensity is generally low in BR_{568}, those modes exhibiting intensity, the 882-cm^{-1} $C_{14}H$ wag and the 830-cm^{-1} lysine-CH_2 wag, are associated with the Schiff base portion of the chromophore. Thus, a study of their Raman intensity should afford quantitative information on the ground → excited state geometry changes that lead to isomerization and proton pumping. The intensities of these modes have been quantitatively studied by Myers et al.[46] The ground → excited state geometry change Δ (in dimensionless normal coordinates) for the 882-cm^{-1} mode is 0.19, indicating a small but possibly significant slope of the excited state surface along the C_{14} HOOP coordinate in the Franck–Condon region. Models for the primary photochemistry which involve a C_{13}=C_{14}-*trans*, C_{14}–C_{15}-*s-trans* → C_{13}=C_{14}-*cis*, C_{14}–C_{15}-*s-cis* isomerization would predict a large Δ in this mode, since the primary structural change involves out-of-plane motion of the C_{14} hydrogen.[47,48]

In summary, the results presented here indicate that the modified Urey–Bradley force field that we have developed for retinals is reliable. By applying the required geometric changes plus relatively modest changes in force constants, we have been able to fit a large body of isotopic data for *all-trans*-retinal,[8] its 13-cis, 11-cis, and 9-cis isomers,[29] the *all-trans*-retinal PSB,[9] BR_{548},[35] and now BR_{568}. If new isotopic data, infrared spectra, or Raman intensities were included in the BR_{568} analysis, the force field could be improved further. Also, it would certainly be possible to refine a different form for the field (e.g., valence) to fit the isotopic data successfully. However, since the magnitude of the isotopic shift of a mode can be quantitatively related to the motion of the labeled atom in that mode,[49] any calculation that successfully reproduces the isotopic shifts must give very similar atomic displacements for the labeled atoms. The success of this calculation on BR_{568} indicates that we can now go on to interpret

(38) Recent studies on retinal Schiff base complexes with Lewis acids [Lopez-Garriga, J. J.; Babcock, G. T.; Harrison, J. F. *J. Am. Chem. Soc.* **1986**, *108*, 7131 and 7241] have led to an alternative analysis of the Schiff base mode in which N—H rock to C=N stretch coupling is not the dominant factor. In this case a similar correlation between the deuteriation-induced shift and hydrogen-bonding environment would be expected. However, it would arise from altered N—H stretch to C=N stretch coupling.

(39) Smith, S. O.; Hornung, I.; van der Steen, R.; Pardoen, J. A.; Braiman, M. S.; Lugtenburg, J.; Mathies, R. A. *Proc. Natl. Acad. Sci. U.S.A.* **1986**, *83*, 967.

(40) Honig, B.; Greenberg, A. D.; Dinur, U.; Ebrey, T. G. *Biochemistry* **1976**, *15*, 4593.

(41) van der Steen, R.; Biesheuvel, P. L.; Mathies, R. A.; Lugtenburg, J. *J. Am. Chem. Soc.* **1986**, *108*, 6410.

(42) Nakanishi, K.; Balogh-Nair, V.; Arnaboldi, M.; Tsujimoto, K.; Honig, B. *J. Am. Chem. Soc.* **1980**, *102*, 7945.

(43) Kakitani, H.; Kakitani, T.; Rodman, H.; Honig, B.; Callender, R. *J. Phys. Chem.* **1983**, *87*, 3620.

(44) Braiman, M.; Mathies, R. *Proc. Natl. Acad. Sci. U.S.A.* **1982**, *79*, 403.

(45) Eyring, G.; Curry, B.; Broek, A.; Lugtenburg, J.; Mathies, R. *Biochemistry* **1982**, *21*, 384.

(46) Myers, A. B.; Harris, R. A.; Mathies, R. A. *J. Chem. Phys.* **1983**, *79*, 603.

(47) Tavan, P.; Schulten, K.; Oesterhelt, D. *Biophys. J.* **1985**, *47*, 415.

(48) Liu, R. S. H.; Mead, D.; Asato, A. E. *J. Am. Chem. Soc.* **1985**, *107*, 6609.

(49) Kitagawa, T.; Nishina, Y.; Kyogoku, Y.; Yamano, T.; Ohishi, N.; Takai-Suzuki, A.; Yagi, K. *Biochemistry* **1979**, *18*, 1804.

vibrational spectra in terms of chromophore structure in other retinal pigments such as rhodopsin, halorhodopsin, and sensory rhodopsin.

Acknowledgment. We thank T. Kitagawa for insightful comments. This research was supported by the National Science Foundation (CHE-8116042), the National Institutes of Health (EY-02051 and GM 27057), the Netherlands Foundation for Chemical Research (S.O.N.), and the Netherlands Organization for the Advancement of Pure Research (Z.W.O.). ^{15}N-BR was generously provided by J. Herzfeld.

Supplementary Material Available: The Cartesian coordinates used in the calculations and a complete description of the force field will be found in Tables XIV and XV (7 pages). Ordering information is given on any current masthead page.

Vibrational Circular Dichroism of Poly(ribonucleic acids). A Comparative Study in Aqueous Solution

A. Annamalai and T. A. Keiderling*

Contribution from the Department of Chemistry, University of Illinois at Chicago, Chicago, Illinois 60680. *Received August 11, 1986*

Abstract: Vibrational circular dichroism data of several synthetic polyribonucleotides have been measured at neutral pH and room temperature in the 1750–1550-cm^{-1} region with sodium cacodylate buffer in D_2O as a solvent and are compared to similar data for monomers and dimers. Polynucleotides studied include homopolymers, some random copolymers, and two double stranded RNAs. The mononucleotides yield no significant VCD whereas, in most cases, the polymers have relatively larger, conservative bisignate VCD signals. The VCD magnitudes of the homodimers, ApA and CpC, are significantly smaller than those of the corresponding polymers but have the same sign pattern. This pattern is consistent with the result of coupled oscillator calculations for these two dimers. VCD of poly(C) has also been measured as a function of temperature and pD. Variation in VCD band shape and magnitude can be correlated to base stacking, base pairing, and degree of order.

Vibrational circular dichroism (VCD) has developed over the past decade from its initial status as an unusual physical phenomenon to one that can be routinely measured on a variety of compounds over a wide spectral range.[1-5] Stereochemists have long appreciated that the multiple, local chromophores accessible with VCD (or the complementary Raman circular intensity differential[2]) offer a potential source of new experimentally derived information about solution-phase molecular conformation. This promise is beginning to be realized via both theoretical and empirical analyses of the spectra.[6-9]

One field of seemingly useful application for VCD is that of biopolymer conformation. Several studies of polypeptide and oligopeptide VCD and the relationship of that data to secondary structure have appeared from our and other laboratories.[9] Until this paper, no parallel work on nucleic acids has appeared. Here we report the first VCD measurements of riboxy-dinucleoside monophosphates and polynucleotides which were made on synthetic samples studied in neutral aqueous solution in the base stretching (C=O, C=C, C=N) region, 1750–1550 cm^{-1}. Our results will be correlated to previous conformational studies on these species.

While extensive use of electronic CD has been made to interpret nucleic acid base stacking, conformational change, and duplex formation,[10] the parallel application of infrared (IR) spectroscopy has been less extensive,[11,12] This perhaps results from the small

(1) Keiderling, T. A. *Appl. Spectrosc. Rev.* **1981**, *17*, 189–226.
(2) Nafie, L. A. In *Advances in Infrared and Raman Spectroscopy*; Clark, R. J. H., Hester, R. E., Eds.; Heydon: London, 1984; Vol. 11, pp 49–93. Nafie, L. A. In *Vibrational Spectra and Structure*; Durig, J. R., Ed.; Elsevier: New York, 1981; Vol. 10, pp 153–225. Nafie, L. A.; Diem, M. *Acc. Chem. Res.* **1979**, *12*, 296–302.
(3) Stephens, P. J.; Clark, R. In *Optical Activity and Chiral Discrimination*; Mason, S. F., Ed.; Reidel: Dortrecht, 1979; pp 263–287.
(4) Mason, S. F. In *Advances in Infrared and Raman Spectroscopy*; Clark, R. J. H., Hester, R. E., Eds.; Heyden: London, 1980; Vol. 8, pp 283–321.
(5) Polavarapu, P. L. In *Vibrational Spectra and Structure*; Durig, J. R., Ed.; Elsevier: New York, 1984; Vol. 13, pp 103–160.
(6) Su, C. N.; Keiderling, T. A. *J. Am. Chem. Soc.* **1980**, *102*, 511–515. Keiderling, T. A.; Stephens, P. J. *J. Am. Chem. Soc.* **1979**, *101*, 1396–1400. Singh, R. D.; Keiderling, T. A. *J. Chem. Phys.* **1981**, *74*, 5347–5356. Singh, R. D.; Keiderling, T. A. *J. Am. Chem. Soc.* **1981**, *103*, 2387–2394. Polavarapu, P. L.; Nafie, L. A. *J. Chem. Phys.* **1980**, *73*, 1567–1575. Marcott, C.; Scanlon, K.; Overand, J.; Moscowitz, A. *J. Am. Chem. Soc.* **1981**, *103*, 483–485.
(7) Freedman, T. B.; Balukjian, G. A.; Nafie, L. A. *J. Am. Chem. Soc.* **1985**, *107*, 6213–6222. Young, D. A.; Lipp, E. D.; Nafie, L. A. *J. Am. Chem. Soc.* **1985**, *107*, 6206–6213. Oboodi, M. R.; Lal, B. B.; Young, D. A.; Freedman, T. B.; Nafie, L. A. *J. Am. Chem. Soc.* **1985**, *107*, 1547–1556.
(8) Polavarapu, P. L.; Nafie, L. A. *J. Am. Chem. Soc.* **1980**, *102*, 5449–5453. Laux, L.; Pultz, V.; Abbate, S.; Havel, H. A.; Overend, J. A.; Moscowitz, A.; Lightner, D. A. *J. Am. Chem. Soc.* **1982**, *104*, 4276–4278. Heintz, V. J.; Keiderling, T. A. *J. Am. Chem. Soc.* **1981**, *103*, 2395–2403. Su, C. N.; Keiderling, T. A. *Chem. Phys. Lett.* **1981**, *77*, 494–499. Su, C. N.; Keiderling, T. A.; Misiura, K.; Stec, W. J. *J. Am. Chem. Soc.* **1982**, *104*, 7343–7344.
(9) Singh, R. D.; Keiderling, T. A. *Biopolymers* **1981**, *20*, 237–240. Lal, B.; Nafie, L. A. *Biopolymers* **1982**, *21*, 2161–2183. Sen, A. C.; Keiderling, T. A. *Biopolymers* **1984**, *23*, 1519–1532. Sen, A. C.; Keiderling, T. A. *Biopolymers* **1984**, *23*, 1533–1545. Narayanan, U.; Keiderling, T. A.; Bonora, G. M.; Toniolo, C. *Biopolymers* **1985**, *24*, 1257–1263. Yasui, S. C.; Keiderling, T. A. *Biopolymers* **1986**, *25*, 79–89. Yasui, S. C.; Keiderling, T. A.; Bonora, G. M.; Toniolo, C. *Biopolymers* **1986**, *25*, 5–15. Narayanan, U.; Keiderling, T. A.; Bonora, G. M.; Toniolo, C. *J. Am. Chem. Soc.* **1986**, *108*, 2431–2437. Yasui, S. C.; Sen, A. C.; Keiderling, T. A.; Toniolo, C.; Bonora, G. M. *Peptides Structure and Function*; Proceedings of the 9th American Peptide Symposium; Deber, C. M., Hruby, V. J., Kopple, K. D., Eds.; Pierce Chemical: Rockford, IL, 1985, pp 167–172. Lipp, E. D.; Nafie, L. A. *Biopolymers* **1985**, *24*, 799–812.
(10) Bush, C. A.; Brahms, J. In *Physico-Chemical Properties of Nucleic Acids*; Duchesne, J., Ed.; Academic Press: New York, 1973; Vol. 2, pp 147–186. Bush, C. A. In *Basic Principles in Nucleic Acid Chemistry*; Ts'o, P. O. P., Ed.; Academic Press: New York, 1974; Vol. II, pp 92–172.
(11) Hartman, K. A.; Lord, R. C.; Thomas, G. J., Jr. In *Physico-Chemical Properties of Nucleic Acids*; Duchesne, J., Ed.; Academic Press: New York, 1973; Vol. 2, pp 1–91. Tsuboi, M. In *Basic Principles of Nucleic Acid Chemistry*; T'so, P. O. P., Ed.; Academic Press: New York, 1974; Vol. I, pp 399–452.
(12) Tsuboi, M.; Takahashi, S.; Harada, I. In *Physico-Chemical Properties of Nucleic Acids*; Duchesne, J., Ed.; Academic Press: New York, 1973; Vol. 2, pp 91–146.

0002-7863/87/1509-3125$01.50/0